

MEASUREMENT OF THE ACTIVATION CROSS SECTIONS OF THE FAST
NEUTRON INDUCED (N,2N), (N,P) AND (N, α) REACTIONS ON THE
ISOTOPES OF MOLYBDENUM, COBALT,
ZIRCONIUM AND GERMANIUM



A THESIS SUBMITTED TO THE DEPARTMENT OF CHEMISTRY,
BANGLADESH UNIVERSITY OF ENGINEERING AND TECHNOLOGY,
DHAKA, FOR PARTIAL FULFILLMENT OF THE REQUIREMENTS FOR
THE DEGREE OF MASTER OF PHILOSOPHY

BY

MD. ABDUL HALIM

EXAMINATION ROLL NO. : 9603213P

SESSION: 1995-96-97



DEPARTMENT OF CHEMISTRY
BANGLADESH UNIVERSITY OF ENGINEERING & TECHNOLOGY
DHAKA, AUGUST, 2003

**BANGLADESH UNIVERSITY OF ENGINEERING AND
TECHNOLOGY, DHAKA**

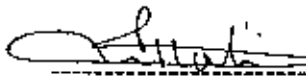
DEPARTMENT OF CHEMISTRY

Certification of Thesis Work

The thesis titled "MEASUREMENT OF THE ACTIVATION CROSS SECTIONS OF THE FAST NEUTRON INDUCED (N,2N), (N,P) AND (N, α) REACTIONS OF THE ISOTOPES OF MOLYBDENUM, COBALT, ZIRCONIUM AND GERMANIUM" submitted by Md. Abdul Halim, Roll No. 960321P, Session 1995-96-97 has been accepted as satisfactory in partial fulfillment for the requirement for the degree of Master of Philosophy on 30 August, 2003.

Board of Examiners

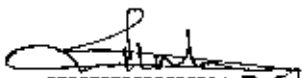
1. **Dr. Md. Rafique Ullah**
Professor
Department of Chemistry
BUET, Dhaka (Supervisor)


Chairman 30/8/03

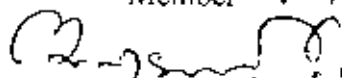
2. **Dr. Rahez Uddin Miah**
Principal Scientific Officer (PSO)
Atomic Energy Research Establishment
Savar, Dhaka (Co-supervisor)

~~Recently Expired~~
Member

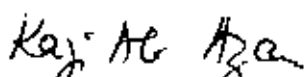
3. **Head**
Department of Chemistry, BUET, Dhaka


Member 30/8/03

4. **Dr. Al-Nakib Chowdhury**
Associate Professor
Department of Chemistry
BUET, Dhaka.


Member 30/8/03

5. **Prof. Kazi Ali Azam**
Department of Chemistry
Jahangirnagar University
Savar, Dhaka.


Member (External) 30.8.2003

DECLARATION

This is to certified that this research work has been carried out by the candidate himself under the supervision of Dr. Md. Rafique Ullah, Professor, Department of Chemistry, Bangladesh University of Engineering & Technology, Dhaka and Dr. Rahez Uddin Miah, Principal Scientific Officer, Institute of Nuclear Science and Technology, Atomic Energy Research Establishment, Savar, Dhaka. The research work presented here is original. No part of this work has been used by anybody for the award of any degree previously



Md. Abdul Halim
Candidate

ACKNOWLEDGMENTS

I would like to express my profound gratitude to my supervisors Prof. Md Rafique Ullah, Department of Chemistry, Bangladesh University of Engineering and Technology, Dhaka, and Dr. Rahez Uddin Miah, Principal Scientific Officer, Atomic Energy Research Establishment (AERE), Savar, for their indispensable guidance, constant encouragement, constructive suggestions and supervision throughout the progress of the work.

I am grateful to Mr. M A Hafiz, Senior Engineer, Dr. S. M. Hossain, Senior Scientific Officer and Kamrun Naher, Scientific Officer, INST, AERE for their friendly cooperation and helpful suggestions at various stages of this work.

I would like to express my sincere gratitude and indebtedness to Dr. Al-Nakib Chowdhury and other teachers of the Department of Chemistry for their keen interest and encouragement during the work. Thanks are also due to all the employees of the Department of Chemistry for their nice cooperation.

I am extremely delighted to express my indebtedness and thankful acknowledgement to Dr. Sk. Md. Yuuns, Principal Scientific Officer and Head, Reactor and Neutron Physics Division, INST, AERE for his constant encouragement and support during the work. Thanks are also extended to all other scientists of the division

I like to thank Mr. Md Ahad Ali, Technical Officer, and Mr Ali Azam, Junior Experimental Officer, for their cooperation in experimental arrangement.

My grateful thanks are due to the authorities of Bangladesh Atomic Energy Commission (BAEC) and BUET for giving me permission for carrying out this M Phil. work and providing financial and technical support.

I wish to express my indebtedness to my wife Syeda Afsarun Nessa for her inspirations and understanding during my study

ABSTRACT

The fast neutron induced cross sections were studied systematically in the energy range 13.90 - 14.80 MeV using the neutron generator facility under identical conditions in order to provide real nuclear data required in the fusion reactor design and in developing semiconductor technology. In the present investigation, the activation cross section data for $^{92}\text{Mo}(n,p)^{92m}\text{Nb}$, $^{94}\text{Mo}(n,2n)^{93m}\text{Mo}$, $^{96}\text{Mo}(n,p)^{96}\text{Nb}$, $^{59}\text{Co}(n,\alpha)^{56}\text{Mn}$, $^{90}\text{Zr}(n,2n)^{89}\text{Zr}$, $^{70}\text{Ge}(n,2n)^{69}\text{Ge}$, $^{74}\text{Ge}(n,\alpha)^{71m}\text{Zn}$ and $^{76}\text{Ge}(n,2n)^{75m}\text{Ge}$ reactions in the neutron energy range of 13.90-14.80 MeV measured in an unified experimental condition. In every case samples of natural abundance was used. Monoenergetic neutrons were produced via $^3\text{H}(d,n)^4\text{He}$ reaction using solid tritium target J-25 neutron generator at the Institute of Nuclear Science and Technology, AERE, Savar, Dhaka with a deuteron energy of 110 keV and steady beam current of 120-130 μA . The different energies of neutrons were obtained as a function of emission angle to the direction of incoming deuteron beam. Activities of the reaction products were determined by measuring the gamma-ray counts of the product nuclei using high resolution HPGe detector gamma-ray spectrometry system. Neutron flux at each sample position was determined by using $^{27}\text{Al}(n,\alpha)^{24}\text{Na}$ monitor reaction with known cross section of the monitor reaction taken from the works of H. Vonach. The experimental values of the cross sections were determined using activation equation. The total uncertainty in cross section was obtained by considering both the statistical errors and possible major sources of systematic errors.

The measured reaction cross section values along with the available literature data have been plotted as a function of neutron energy to get the excitation functions of the reactions. The theoretical cross section calculations using statistical code SINCROS-II in the energy range 13 to 15 MeV were performed to validate the experimental data theoretically. Measured data will help to remove existing discrepancies in the cross section values, will offer substantial nuclear data base for fusion reactor design, current evaluations of neutron activation cross section and nuclear model calculation for nuclear technology application.

CONTENT

	Page No
ABSTRACT	
CHAPTER 1 GENERAL INTRODUCTION	1
1.1 Neutron Sources	4
1.2 Status of Neutron Cross Section Data for Mo, Co, Zr and Ge	5
1.3 Aim and Scope	6
CHAPTER 2 GENERAL EXPERIMENTAL	
2.1 General Consideration of Neutron Activation Analysis	11
2.2 Instruments and Techniques for Production of Neutrons	13
2.2.1 Production of Fast Neutron by J-25 Neutron Generator	13
2.2.2 Organization of Neutron Generator	15
2.2.2.1 Positive ion Source	17
2.2.2.2 Vacuum System	17
2.2.2.3 Accelerator Tube	17
2.2.2.4 Quadrupole Lens	18
2.2.2.5 High Voltage Generator	19
2.2.2.6 Tritium Target	19
2.2.2.7 Neutron Monitor	20
CHAPTER 3 GAMMA-RAY SPECTROMETRY SYSTEM	22
3.1 Interaction of Gamma-ray with Matter	22
3.1.1 Photoelectric Effect	22
3.1.2 Compton Scattering	24
3.1.3 Pair Production	25
3.2 Detection and Measurement of Gamma-rays	29
3.2.1 High Purity Germanium (HPGe) Detector	30
3.2.2 High Voltage Power supply	32
3.2.3 Preamplifier	33

3 2 3	Amplifier	34
3 2 4	Multichannel Pulse Height Analyzer	34
3 3	Energy Calibration of the MCA	35
3 4	Measurements of Detector Parameters	37
3.4.1	Energy Resolution	37
3.4.2	Efficiency Measurement	38
3 4 3	Background Radiation	39
3.4 4	Shielding Arrangement of the Detector	40

CHAPTER 4 MEASUREMENT OF (n,2n), (n,p) AND (n, α) REACTION CROSS SECTIONS ON THE ISOTOPES OF Mo, Co, Zr AND Ge IN THE NEUTRON ENERGY RANGE 13.90 – 14.80 MeV 41

4.1	Measurement of Cross Sections for Molybdenum and Cobalt Isotopes	41
4.2	Measurement of Cross Section for Zirconium and Germanium Isotopes	45

CHAPTER 5 NUCLEAR CROSS SECTION CALCULATION SYSTEM WITH SIMPLIFIED INPUT FORMAT, VERSION-II (SINCROS-II)

		53
5.1	Composite of SINCROS-II	54
5 2	Input and Output Format of EGNASH2	54
5 3	Optical Model Potential Parameters	55
5.4	Parameters for Level Density and Gamma-ray Transition	56
5.5	Determination of the Value of Parameters	58
5.6	Parameter Determination of the Pre-equilibrium Process	58
5 7	Parameter Determination of the Level Density	58

CHAPTER 6 RESULTS AND DISCUSSION 60

6 1	The $^{92}\text{Mo}(n,p)^{92m}\text{Nb}$, $^{94}\text{Mo}(n,2n)^{93m}\text{Mo}$ and $^{96}\text{Mo}(n,p)^{96}\text{Nb}$ Reaction	60
6.2	The $^{59}\text{Co}(n,\alpha)^{56}\text{Mn}$ Reaction	62

6.3	The $^{90}\text{Zr}(n,2n)^{89}\text{Zr}$ Reaction	63
6.4	The $^{70}\text{Ge}(n,2n)^{69}\text{Ge}$ Reaction	65
6.5	The $^{74}\text{Ge}(n,\alpha)^{71\text{m}}\text{Zn}$ Reaction	67
6.6	The $^{76}\text{Ge}(n,2n)^{75\text{m-}}\text{Ge}$ Reaction	67
CHAPTER 7 REFERENCES		69
APPENDICES		73

CHAPTER 1
GENERAL INTRODUCTION

CHAPTER 1

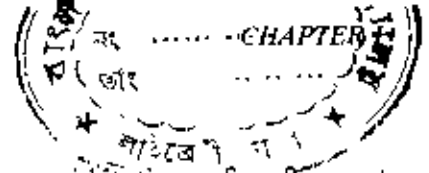
GENERAL INTRODUCTION

Neutron has been playing an important role in the study of nuclear reactions, nuclear structure and in the basement and advancement of nuclear technology since the discovery of its by Chadwick in 1932. A detailed study of nuclear reactions is one of the largest areas of nuclear chemistry and physics. This field of study originated when Rutherford investigated the scattering of low energy particles in a thin gold foil in 1911.

Radioactivities produced in structural materials with neutrons as well as with charged particles are of immense importance in the whole range of nuclear applications. A particular structural material may be consisted of many stable isotopes. Fast neutrons, therefore, lead to the formation of many radioactive products. Therefore an accurate knowledge of their formation cross sections is important for estimating the total induced activity. A study of (n, charged particle) reactions on the structural materials is of great importance since such reactions give rise on the one hand to transmutation products which might strongly influence the development of damage microstructure and thereby lead to property changes and on the other to hydrogen and helium gases which may cause high temperature embattlement of structural materials¹. The experimental data, generally obtained via the activation technique, are rather discrepant²⁻⁴

In figures 1.1 and 1.2 are shown two possible designs of future Tokamak-type fusion reactors. Figure 1.1 shows plasma composed of deuterons and tritons surrounded by a first wall of toroidal shape which in turn is surrounded by a shielding blanket in which, through interaction of the neutrons produced in the plasma with lithium, tritium, is produced. Figure 1.2 shows a complete design of a possible fusion reactor along with heat exchanger and other components. It also shows how tritium is fed back into the plasma.

Developing a material suitable for the first wall and similar critical locations is one of the most difficult problems of fusion. Present materials fail in their resistance to radiation damage, creep and other things to meet the lifetime requirements of a fusion



reactor by about an order of magnitude; ingenious considerations for frequent replacement present cost penalties. Thus materials development will be a critical pacing item in the future fusion programme⁵.

The deuterium and tritium in the plasma react according to the scheme

$D + T \rightarrow ({}^4\text{He} + 3.25 \text{ MeV}) + (n + 14.1 \text{ MeV})$. The helium ion deposits its energy in the plasma thereby keeping the plasma hot. The neutron deposits its energy in the blanket that surrounds the discharge plasma. The blanket not only absorbs the 14 MeV neutron energy, but produces an additional 9.2 MeV of energy per incident neutron. In addition the neutron reactions with the natural lithium in the flibe, together with the neutron multiplication reactions in the beryllium⁶, easily produce a tritium breeding ratio of 1.04.

The details of compilation of several types of cross sections used in the nuclear heating calculation are described elsewhere⁷. The distribution of tritium production reaction rates i.e., the tritium breeding ratio by ${}^6\text{Li}(n,\alpha)t$ reaction is 0.80 and the tritium breeding ratio by ${}^7\text{Li}(n,n'\alpha)t$ reaction is 0.36. The neutron flux at the first wall was calculated as $6.3 \times 10^{13} \text{ n cm}^{-2} \text{ s}^{-1}$ for 14 MeV, $1.96 \times 10^{14} \text{ n cm}^{-2} \text{ s}^{-1}$ for $E > 0.1 \text{ MeV}$ and $2.7 \times 10^{14} \text{ n cm}^{-2} \text{ s}^{-1}$ for total neutron. Difference of reaction rates between the plasma and coolant sides of the first wall are about 10% for both (n,α) and (n,p) reactions⁸. Since radiation damage can cause reduction in strength and ductility, appropriate evaluation of the irradiation behavior of the wall material is of major importance in the design study.

The interaction of radiation with crystalline solids has been studied extensively in the last two decades, mainly as a result of the development of nuclear energy. For non-fissionable metals major attention must be paid to those types of radiation that are able to displace atoms from their normal lattice positions. In this respect irradiation with high energetic particles such as fast electrons, neutrons, protons, deuterons and ions are to be considered. More indirectly, thermal neutron irradiation and α -irradiation may also cause atomic displacements. Transmutation elements resulting from nuclear reactions may in some cases be important too⁹. In recent years increasing attention has

also been paid to the effect of spontaneous recombination between vacancies and interstitial, occurring even at very low temperature. Theoretical and experimental work, as well as computer work in this field, have contributed to a better understanding of the damage production mechanisms¹⁰⁻¹⁶.

The accurate knowledge of neutron interaction cross section around 13-15 MeV energies are of significant interest for fusion facilities. In D-T fusion almost 80% of the total energy is carried off by 14 MeV neutron¹⁷. In fusion reactor, the 14 MeV neutrons produced in the plasma are slowed down in the first wall and in the blanket. A typical spectrum of the neutrons entering the blanket extends down to keV energies, with the bulk of the neutrons centered in the MeV region and a strong component of 14 MeV neutrons. For neutronic calculations therefore all neutron cross sections of the fusion reactor materials have to be known from keV energies to about 15 MeV, with an emphasis on partial reactions such as (n,p), (n,np), (n, α), (n,n α), (n,2n) etc. and on energy and angular distribution of secondary particles (neutrons and charged particles) emitted in these reactions.

The (n,xn), ($x \geq 2$) and (n,l) reactions can be used to enhance the neutron flux through neutron multiplication. In normal D-T fusion reactors, materials with high (n,2n) cross sections are used as main or additional materials in the first wall. They can lead to a significant multiplication of the neutrons impinging on the blanket. These neutrons enhance tritium breeding. Because of the Coulomb barrier, the emission of neutrons is more likely than that of charged particles. Neutrons captured in (n,p), (n, α), as well as (n, γ), (n,d), (n,t) and (n,³He) reactions with lower cross sections are not available for tritium breeding. Major parasitic neutron absorbers are the structural materials used in the first wall and in the blanket through (n,p) and (n, α) reactions.

14 MeV neutrons have a rather singular threefold importance:

- (1) They represent about the upper energy limit of neutrons occurring in nuclear fission reactors

- (2) The D-T reaction in which 14 MeV neutrons are generated represents the basis for all contemporary fusion reactor designs based on magnetic plasma confinement.
- (3) The D-T reaction used in neutron generators allows the measurements of 14 MeV neutron cross sections.

Now a days, neutron production from plasma is a reality, which makes the nuclear data specially useful in monitoring plasma temperature and assessing D-T fuel "burn" rates during the containment intervals. For blanket design purpose, tritium breeding cross sections and neutron multiplier cross sections for energies of about 14 MeV and below are important. Radiation damage by energetic neutrons and long-lived activation of fusion reactor structure are also important. These are the affects which will influence the longevity and service of reactor facilities.

Since 14 MeV neutrons dominate the neutron field around D-T plasma, the accuracy of the cross section data at 14 MeV neutrons are important for the prediction of reactor parameters such as tritium breeding, nuclear heating, radiation damage, radioactive waste estimation, calculation of the activation in materials to be used in fusion reactors and so on. Hence nuclear data have a vital role to play in nuclear science and technology. To date there has been enormous advancement in the field of nuclear data measurement, evaluation and nuclear reaction theory as well as applications. The want of nuclear data, particularly nuclear cross sections have been increased during the last three decades. Measurements, calculation and evaluation of these cross sections have been extensively undertaken during these days. Herein are described some fundamentals pertaining to the present investigation.

1.1 Neutron Sources

Recently, much progress has been made in the production of intense neutron sources. The availability of neutron sources with well defined characteristics is essential for a detailed study of neutron induced reactions. The neutron sources are categorized as

monoenergetic and continuous (white neutron sources) sources. There are three principal methods for producing neutrons. These are

- 1) interaction of alpha or gamma radiation from radioactive substances with light elements like Be
- 2) reaction of accelerated charged particles from accelerators with light nuclei
- 3) fission reactor

The first and third methods produce neutrons of continuous energy. The production of monoenergetic neutrons is achieved by second method

Different types of neutron generator producing mono-energetic neutrons through D-D and D-T reactions are used in many laboratories around the world with a view to facilitating research on nuclear reactor technology. A SAMDES J-25 AID (France) Neutron Generator was installed at the Institute of Nuclear Science & Technology(INST), Atomic Energy Research Establishment (AERE), Savar, under the coordinated research program with the International Atomic Energy Agency (IAEA) for the measurements of nuclear data. In J-25 neutron generator, 14 MeV mono-energetic neutrons are produced via ${}^3\text{H}(d,n){}^4\text{He}$ reaction. The large positive Q-value¹⁸ (17.6 MeV) and low atomic number makes it possible to produce 14 MeV neutrons even at low deuteron incident energies, e.g., $E_d = 100\text{-}200$ keV. This intense neutron source is, therefore, used for the investigation of the interaction of fast neutrons with structural materials of nuclear reactors which are important for design, development, safe operation of fission and fusion nuclear reactors. In activation measurements, monoenergetic neutron sources are needed since the determination of cross section is energy dependent. Therefore in this work, only neutrons produced from the reactions of accelerated charged particles are discussed further in the latter section.

1.1 Status of Neutron Cross Section Data for Mo, Co, Zr and Ge

A detailed survey of literature shows that the ample cross section data of the $(n,2n)$, (n,p) and (n,α) reactions on the isotopes of molybdenum, cobalt, zirconium and germanium in the energy range of 13-15 MeV are not that available. S. M. Qaim et

al.²⁶ measured the excitation functions for (n,p) reaction on ⁷⁰Ge, ⁷³Ge and ⁷⁴Ge isotopes in the neutron energy range of 6.2 to 12.4 MeV. R. U. Miah¹⁹ measured the cross sections of (n,2n) reactions on ⁹⁶Mo, ⁹⁰Zr, ⁷⁰Ge and ⁷⁶Ge isotopes and (n,p) reaction on ⁹²Mo, ⁹⁶Mo isotopes and (n,α) reaction on ⁷⁴Ge isotopes in the energy range of 13.64 -14.71 MeV. R. U. Miah also performed the theoretical calculation of cross sections of ⁷⁶Ge(n,2n)^{75m+g}Gc reactions using statistical code EXIFON²⁰. Wenrong et al.²¹ reported both the measured and evaluated cross section data for (n,2n) reaction on ⁹⁰Zr isotopes in the energy range of 13 to 15 MeV. Recently, Cullen et al.²², Bychkov et al.²³, Ikeda et al.²⁴ and G. Erdtman²⁵ reported neutron activation cross section on the selected reactions. In most cases, it has been shown a significant deviation in cross section data measured / evaluated by different authors for the same reaction. S. M. Qaim²⁶ reported the cross section of ⁹⁸Mo(n,p)⁹⁸Nb at 14.7±0.3 MeV to be 2.6±0.7 mb whereas C. V. S. Rao et al.²⁷ reported this cross section to be 10.0±1.2 mb. Both of them used activation technique. Similarly in the measurement of cross section of ⁹⁰Zr(n,2n)⁸⁹Zr reaction, a cross section value of 517±47 mb was reported in CIND²⁸ whereas Y. Fujino²⁹ reported the value to be 805±58 mb. The main sources of the discrepancy in the experimental data arise from the difference of the experimental conditions, neutron source characterization, radiation measuring technique, neutron monitoring method, standard cross section data and nuclear data (gamma-ray, half life, natural abundance) used to deduce the final data. Although extensive data for (n,2n), (n,p) and (n,α) reactions on various nuclides at 13-15 MeV neutron energy are found in the literature, many of them appear to contain relatively large systematic errors and needs further evaluation.

1.2 Aim and Scope

Extensive measurements of fast neutron induced reactions cross sections on structural materials of fission and fusion reactors have been carried out during the last years at several laboratories over the neutron energy range from threshold up-to 15.0 MeV. There is high demand of precision cross section data for engineering requirements as well as for validation support of nuclear model calculations.

The prediction of atomic displacement rates and helium production rates requires knowledge of the cross sections of the nuclear reactions on the isotopes of structural materials. In addition nuclear power engineering needs, based on fission reactors, many other regions of science and technology have very large needs in nuclear cross section data.

Semiconductor electronic components are sometimes needed to be used in intense fast neutron fields for nuclear measurements. There are many semiconductors available, but very few of them have practical application in electronics. Germanium is the most frequently used semiconductor material. It is because the energy required to break their covalent bond (i.e., energy required to release an electron from their valence bonds is very small; being 0.7 eV) Germanium has become the model substance among the semiconductors because it can be purified relatively well and crystallized easily. Therefore, the investigation of fast neutron interactions with atomic nuclei of this semiconductor material would yield important information to the study of nuclear structure and reaction mechanism and provide a good way of testing the application of nuclear models. From the view point of semi-conductor technology, neutron activation cross section data around 14 MeV have also become important specially for calculations on nuclear transmutation rate, induced activity, radiation damage and so on. Such data are also needed for further improvement of semi-conductor technology. The cross sections of the neutron induced reactions for Ge isotopes are of some interest, both from the fundamental point of view and for estimating radiation damage in semi-conductor materials.

New regions of nuclear data applications appeared for example such as nuclear safety, alternative reactors, space reactors, industrial applications, decommissioning of long time operated fission reactors, high energy neutron dosimetry which widen the needs for nuclear data both in energy range and number of reactions. To meet these needs the experimental and theoretical investigations are made of radiation interactions with nuclei in many countries and during long period of time.

The results of intensive activity of nuclear scientists allowed to meet many requirements, but nevertheless the present and future requirements put new tasks both in increasing nuclear cross section data amount and improving reliability and accuracy of evaluated data. It can be mentioned that the uncertainties in nuclear data lead to uncertainties in the prediction of reactor parameters. Large uncertainties in turn lead to the large and expensive margins in design.

In view of these consideration, we intend to carry out a piece of research work on the measurements of excitation functions of the reactions $^{92}\text{Mo}(n,p)^{92m}\text{Nb}$, $^{94}\text{Mo}(n,2n)^{93m}\text{Mo}$, $^{96}\text{Mo}(n,p)^{96}\text{Nb}$, $^{59}\text{Co}(n,\alpha)^{56}\text{Mn}$, $^{90}\text{Zr}(n,2n)^{89}\text{Zr}$, $^{70}\text{Ge}(n,2n)^{69}\text{Ge}$, $^{74}\text{Ge}(n,\alpha)^{71m}\text{Zn}$ and $^{76}\text{Ge}(n,2n)^{75m+g}\text{Ge}$ in the energy range of 13.90 to 14.80 MeV in the same experimental configuration. The cross sections of this reaction in this energy region were also determined theoretically by using statistical code SINCROS-II³⁰ to validate the experimental data.

Activation cross section data in the neutron energy range 13 - 15 MeV, as mentioned earlier, are needed primarily for the engineering design of fusion reactors, especially for the calculations of tritium breeding, radiation damage, radiation shielding, induced activity, nuclear heating and so on. But there are other important applications of 14 MeV cross section data. These are investigation of nuclear theories and nuclear structures, testing of nuclear models, neutron dosimetry, isotope production, mineral exploration, fast neutron activation analysis and so on.

Zirconium, molybdenum and cobalt are the most important constituents of the fusion structural materials^{31,32}. Germanium is the important semiconducting material. A critical survey of the available literature reveals that some information of the cross sections of the selected reactions have been existed. However, for more information and better understanding on the field extensive research work are still inevitable. The present measurement aims at adding some newer data points to the existing literature.

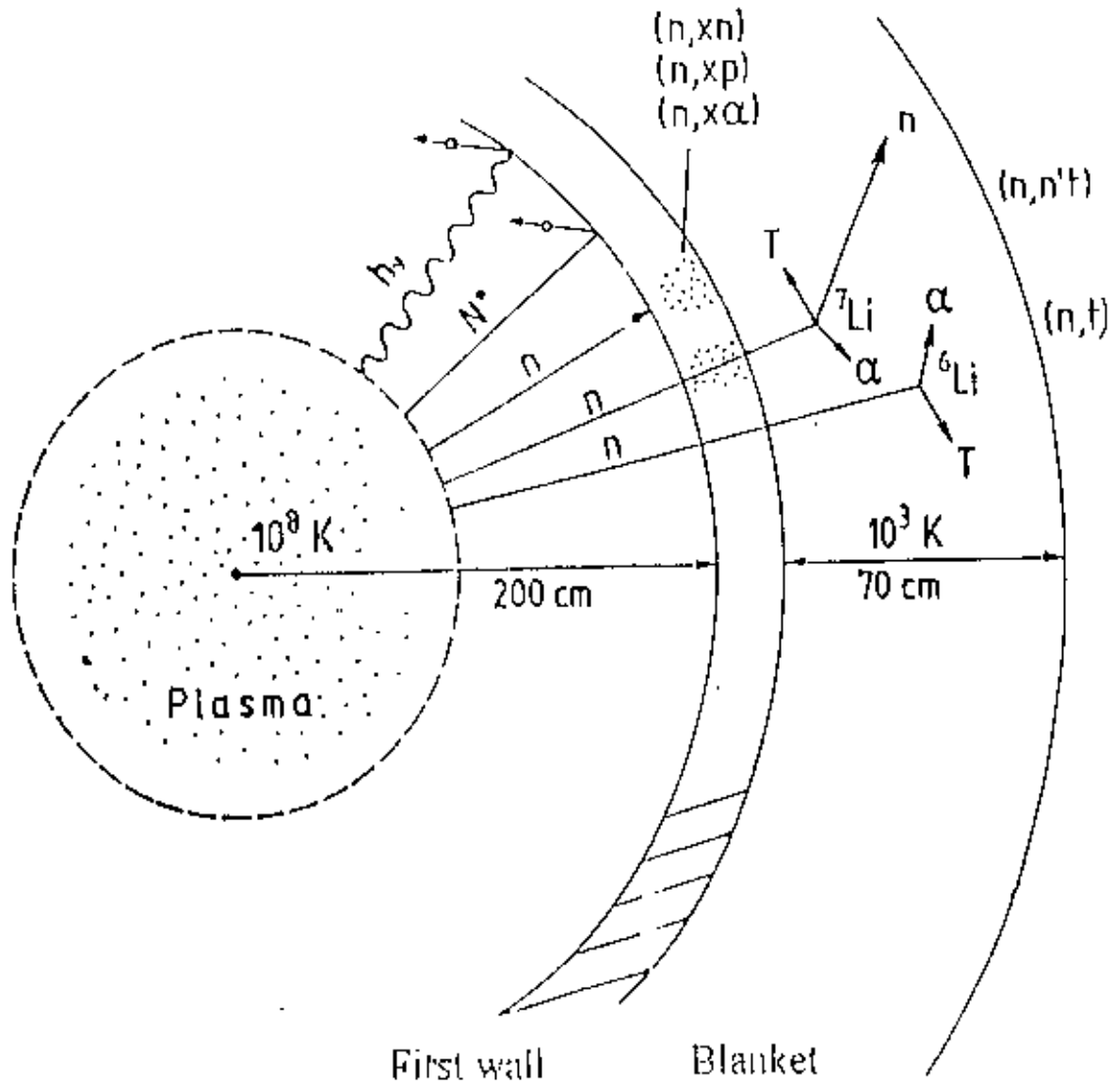


Fig. 1.1 Scheme of a possible tokamak-type fusion reactor. Major reactions occurring in the first wall and blanket are shown.

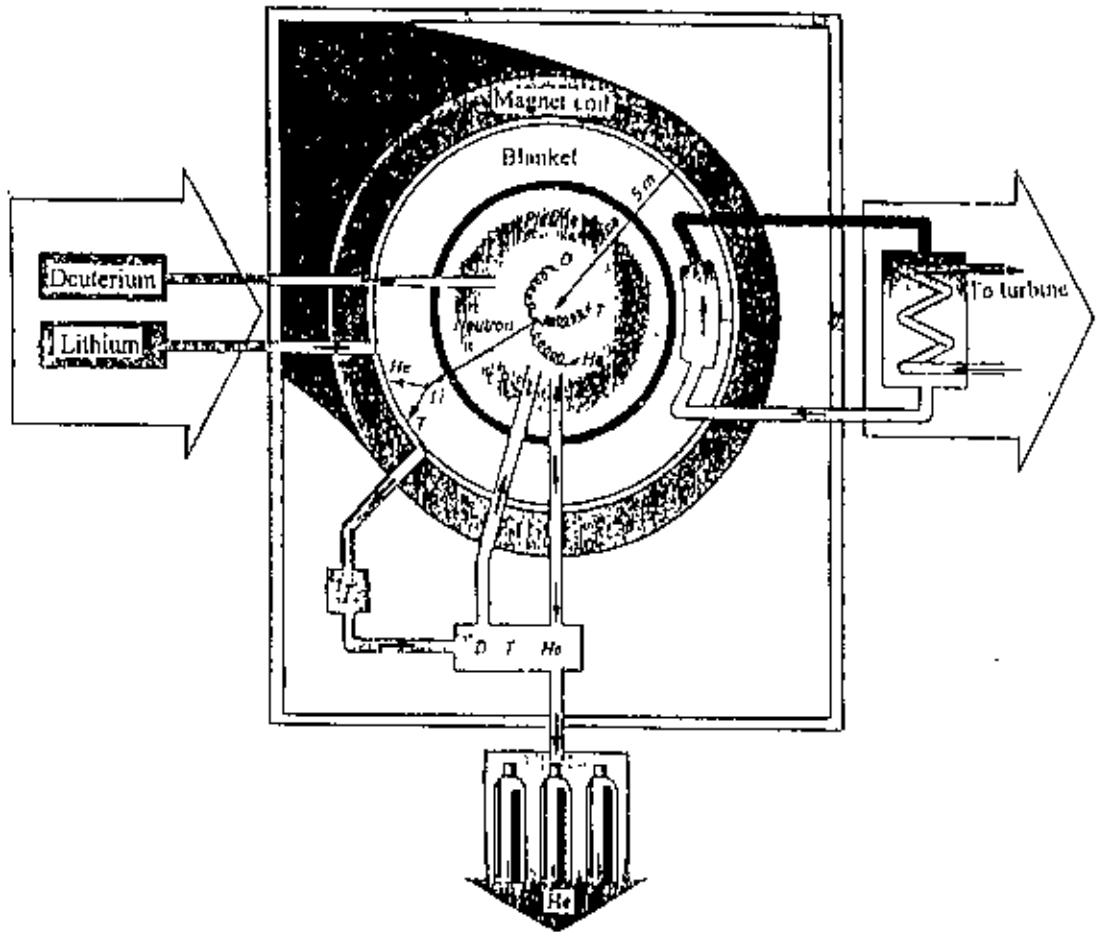


Fig. 1.2. Complete design of a possible fusion reactor.

CHAPTER 2
GENERAL EXPERIMENTAL

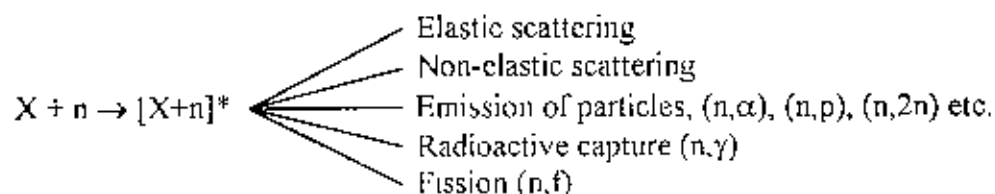
CHAPTER 2

GENERAL EXPERIMENTAL

2.1 General Consideration of Neutron Activation Analysis (NAA)

The method of activation analysis depends upon the formation of radio nuclides from elements in the sample when they are subjected to bombardment with energetic particles, such as neutrons, photons, deuterons, α particles etc. Thus the process in which the sample is subjected to nuclear bombardment and then analyzed for its radio active contents, is known as activation analysis. Thermal neutrons are particularly suitable, because many elements have high thermal neutron absorption cross sections, but 14 MeV neutrons have grown in importance, because the ease with which they can be produced by low voltage accelerators and their effectiveness in the detection of trace elements such as N, O, Si, P, Ti and Pb, which are difficult or impossible to detect with thermal neutrons. Neutrons with selected energies between thermal and 14 MeV are also helpful for emphasizing some elements in the presence of others which perhaps are present in greater concentration³³. Based on highly characteristic and well defined nuclear properties of the elements, this technique is close to an ideal non-destructive analytical method, capable of handling samples in liquid, solid or powder form.

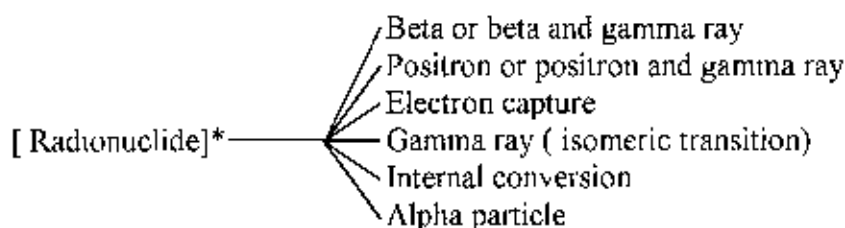
Neutron activation is a nuclear reaction phenomenon. When a neutron interacts with a target nucleus, a compound nucleus is formed. De-excitation of the compound nucleus can occur in different ways that are independent of the way the compound nucleus is formed. Each of these processes (shown below) has a certain probability, depending on the nuclear cross section of each mode, which is related to the excitation energy of the compound nucleus³⁴.



In elastic scattering the resulting nucleus is identical with the target, whereas in non-elastic scattering a radioactive isomer may be formed. In the emission of particles the

resulting nuclide is usually radioactive and differs from the target nuclide in atom or mass number or both. The most favorable and important nuclear reaction in NAA is radioactive capture (n, γ), in which the excited nucleus passes to a lower energy state by the emission of one or more γ -rays. The resulting nuclide is usually radioactive. In fission the excited nucleus splits into two nuclei accompanied by the emission of the neutrons and γ -rays. The fission process is limited to only a few elements with high atomic numbers ($Z > 90$), thus its significance in NAA is very limited.

A radioactive nuclide has a characteristic half-life ($t_{1/2}$), mode of decay and energy of emitted radiation during the decay process. Depending on the energy considerations (Q value), a radionuclide can decay to a daughter product (usually stable) by various ways, as shown below.



In neutron activation analysis, neutrons are used to activate target nucleus. The neutron may be regarded as to be captured by atomic nucleus to give a large nucleus with the same positive charge, which is, therefore, an isotope of the element. Nuclei, which have been excited or activated by neutron capture, give characteristic gamma rays by which it is possible to identify the nuclei. The half life periods of various isotopes formed in this manner from various elements will be widely different and this constant (i.e., half life period) may be used in the identification of active isotopes along with other pertinent information in many instances. In activation analysis, activation and spectrometry take place separately.

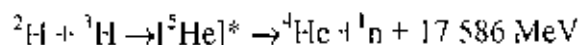
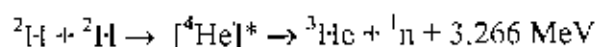
Most of the radio-nuclides that undergo decay by alpha, beta or positron emission and by electron capture also emit gamma rays as a result of readjustment of energy content in the radio-nuclides during their transition from excited states to more stable states. Gamma-ray measurements have, in general, much wider applications in NAA because gamma-rays emitted from the most radio-nuclides have a wider range of energies (10-

3000 keV) and have large penetrating range. They are subject to minimal loss by absorption in a sample matrix during their measurements. This property coupled with the developments in high resolution and high efficiency semiconductors. For example High Purity Germanium (HPGe) detectors and availability of high neutron flux reactors, neutron generator, etc., make NAA gamma spectrometry a powerful technique in measuring activation cross section and multi-elemental determination.

2.2 Instruments and Techniques for Production of Neutrons

2.2.1 Production of Fast Neutron by J-25 Neutron Generator

The two nuclear reactions used for the production of fast neutrons by low-voltage accelerators can be expressed as follows:



At acceleration voltages used in neutron generator of about 150 to 200 keV, the cross section for the D-D reaction is about 3×10^{-26} cm²/atom. Whereas, for thin targets, the D-T cross section at about 150 keV incident deuteron energy is about 4.55×10^{-24} cm²/atom and the maximum value 5 barns are shown at 110 keV incident deuteron bombarding energy³⁵. From cross section considerations, it would be expected that at 150 keV incident deuteron energy, the output from the D-T reaction would be about 300 times greater than that from the D-D reaction. Therefore, the contribution of the D-D background neutrons to those emitted in the D-T reaction can be neglected. Experimentally, it has been observed that this improvement is indeed approximated for thick target neutron production. The prolific yield from the D-T reaction makes it particularly useful for analytical applications requiring a high degree of sensitivity; however, the D-D reaction is sometimes preferred in special cases because of minimization of the number of interferences. Neutron sources based on the light particle reactions have played an important role in experimental fast neutron research^{36,37}. Henceforth 14 MeV neutrons from neutron generator were used in the present investigation although various kinds of neutron sources with different energy ranges

and intensities are available³⁸ Using low-energy accelerators, monoenergetic neutrons are generally produced by the "big-4" reactions shown in Table 2.3.

Table 2.1 Data of the "big-4" neutron source reactions.

Reaction	Q-value (MeV)	Breakup reaction	Breakup threshold (MeV)	Monoenergetic neutron energy range (MeV)
${}^3\text{H}(d,n){}^4\text{He}$	+17.590	$\text{T}(d,np)\text{T}$ $\text{T}(d,2n){}^3\text{He}$	3.71	11.75 - 20.5
${}^2\text{H}(d,n){}^3\text{He}$	+3.270	$\text{D}(d,np)\text{D}$	4.45	1.65 - 7.75
${}^3\text{H}(p,n){}^3\text{He}$	-0.763	$\text{T}(p,np)\text{D}$	8.35	0.3 - 7.6
${}^7\text{Li}(p,n){}^7\text{Be}$	-1.644	${}^7\text{Li}(p,n){}^7\text{Be}^*$	2.37	0.12 - 0.6

The production of neutrons by bombarding suitable targets with the isotopes of hydrogen is particularly attractive since the net energy gain by the reaction system is quite large. For instance, a proton entering a nucleus adds about 8 MeV of energy to the system. In the case of an α -particle, the net gain is not quite as much since the difference between approximately 28 MeV of binding energy required to break up an α -particle into two neutrons and two protons and the 32 MeV gained by the reaction system from the addition of four extra nucleons, is only 4 MeV. When compared with the entry of a deuteron, however, even the energies brought in by protons and α -particles are considered small. The deuteron requires only 2 MeV to split into a neutron and a proton but adds 16 MeV into the reaction system, a net gain of 14 MeV.

In the present experiment, reaction (2) was used to produce monoenergetic fast neutron. To take place this reaction (2), the J-25 neutron generator was so designed that deuterium molecules are ionized in the ion source bottle, accelerated in an electrostatic field of 110 keV at a beam current of 200 μA and focused on a tritium target. The deuteron interacts with tritium in the target to form a compound nucleus [${}^5\text{He}$]* at a highly excited state which later breaks down into a ${}^4\text{He}$ nucleus and a neutron with the release of 17.6 MeV energy.

The reaction $T(d,n)^4\text{He}$ has a positive Q -value of 17.6 MeV. Q -value means the energy released or absorbed in a reaction. An amount of energy equal to the Q -value of the reaction plus kinetic energy of the incident particle (${}^2\text{H}^2$) is shared by the outgoing particle (${}^1\text{n}$) and residual nucleus (${}^4\text{He}$). The fraction of the energy which each of them receives can be determined by applying the principle of conservation of energy and momentum. However, the lighter particle always takes the greater portion of the available energy. A neutron emitted in the forward direction carries away about 14.1 MeV of the energy. The remaining 3.5 MeV appears as the kinetic energy of the alpha-particle. The alpha particles are absorbed in the target holder but the neutrons being very penetrating, escape into the room. For 110 keV deuteron, the D-T source properties were studied earlier¹⁹ at the J-25 neutron generator facility, INST, AERE, Savar, Dhaka. The energy of the neutrons in the center of mass system is 14.1 MeV. In the laboratory system the neutron energy varies from 14.71 MeV at 0° to 13.55 MeV at 180° .

2.2.2 Organization of Neutron Generator

Neutron generators are small accelerators consisting of vacuum, magnetic, electrical and mechanical components, radiation sources, cooling circuits and pneumatic transfer systems. There are various types of ion sources, beam accelerating and transport systems, targets, high voltage and other power supplies, neutron and tritium monitors and shielding arrangements. The general characteristics of the neutron generator is given in Table 2.2 and a partial view of the J-25 Neutron Generator is shown in Figure 2.2.

Table 2.2 General characteristics of J-25 neutron generator

Model	J-25
Maximum high voltage	150 kV
Maximum current	2.5 mA
Power consumption	5 kVA
Neutron production	D-T Reaction
Neutron energy	13-15 MeV
Maximum neutron yield	2×10^{11} n cm ⁻² sec ⁻¹

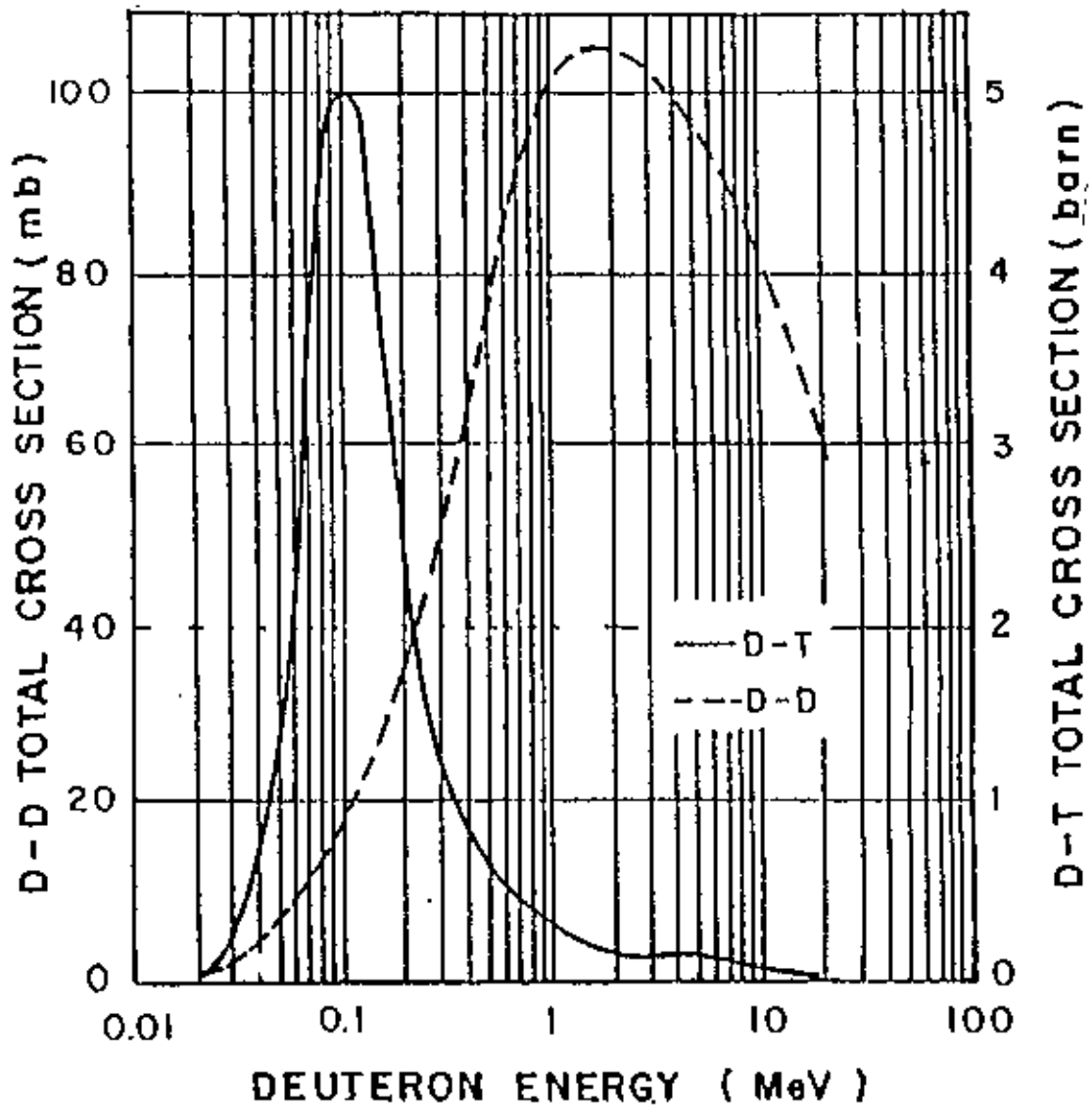


Fig. 2.1 Cross section of D-D and D-T reactions as a function of deuteron energy¹⁷

The major components of the neutron generator are briefly described below

2.2.2.1 Positive Ion Source

The radio frequency (RF) type ion source is used to produce deuteron ion. The deuterium gas is fed at a controlled rate into the glass envelope via a gas leak. If an RF voltage is applied across the exciter rings, an electrical field is generated between the two ring electrodes located outside and in contact with the glass envelope. Since glass is an insulator, the electric field lines traverse the glass and pass into the gas. The power supplied to the RF oscillator is adequate to create and maintain intense ionization of the gas. This gas discharge glows with a bright pink color. The plasma color (a bright pink) is also one of the principal guides to the performance of the source. If a DC potential is now applied across the bottle, ions can be directed toward the exit canal of the bottle. A gap or electrostatic focusing lens is used to prevent the divergence in exit canal and directs the ions into the accelerating section of the generator. The ions enter the field of the acceleration tube where they are accelerated through a potential of 110 kV.

2.2.2.2 Vacuum System

The aim of all vacuum systems for a neutron generator, as for a charged particle accelerator, is that the accelerated deuteron ions should reach the tritium target without collision with gas molecules. To do this, it is necessary to keep the pressure in the accelerating tube so low that the mean free path of air molecules should exceed the length of the accelerating tube. The vacuum system of the neutron generator consists of a dipstick pump of EDWARDS high vacuum, England. The pressures of different mean free path are shown in Table 2.2

2.2.2.3 Acceleration Tube

The intense ion plasma produced inside the ion source is directed through the exit canal and into the focusing and accelerating sections of the neutron generator. Generally, these functions take place in a single tube composed of 10 electrodes and a hollow

cylindrical insulators of ceramic. The insulators and the metal electrodes are bonded together with polyvinyl alcohol (PVA) glue to form vacuum tight (joints). It has permitted the dual action of focusing and acceleration. An equal division of the high voltage (110 kV) is performed for the whole length of the tube. As a result the beam receives a kick of 11 kV in passing each electrode. The focusing electrodes carry a negative DC potential with respect to the terminal high voltage (110 kV) applied to the first accelerating stage. By utilizing a system of resistors a potential difference is maintained between each accelerating stage. This division of high voltage can be evenly distributed between the individual stages so that the ion beam receives a boost in energy equivalent to the potential drop at each stage. At the end of the accelerating tube the ions have acquired an energy equivalent to the total potential drop between the high-voltage terminal and ground. The positive ion beam reaches the target with an energy equal to their charge multiplied by the potential difference through which they have fallen and thus a continuous deuteron beam of 110 kV energy is obtained.

Table 2.3 Mean free path vs. pressure¹⁹

Pressure (mbar)	Mean free path (cm)
atmospheric	6×10^{-6}
1	5×10^{-3}
10^{-3}	5×10^0
10^{-6}	5×10^2
10^{-9}	5×10^6

2.2.2.4 Quadrupole Lens

Electrostatic (or magnetic) quadrupole lenses are commonly used as post-acceleration ion beam lenses at almost all accelerators. Electrostatic quadrupole lenses are more simple, but they need power and high voltage feed through into the vacuum system. Furthermore a high vacuum is required in the system to avoid corona discharges. Quadrupole lens consists of four hyperbolically shaped pole faces or electrodes. The quadrupole lens focuses in one plane and defocuses in the perpendicular plane. Thus several such lenses must normally be combined to make a useful lens system. Usually

quadrupole doublets and triplets are in use at neutron generators. The biased quadrupole lens is powered asymmetrically, so that the particle beams are focussed and steered. The biased quadrupole lens requires split power supplies.

2.2.2.5 High Voltage Generator

High voltage generators are used in neutron generators for excitation, focusing acceleration, etc. of the deuteron ions. It has the following main components:

Rotor

Ionize electrodes

Inductors.

The rotor, which is a tube-like cylinder, made of insulating material. The rotor is driven by an electric motor and charges are deposited on the surface of the rotor. The rotating cylinder is the only moving part of this electrostatic generator.

The ionize electrodes, which are very thin metallic needles (blades) placed in close proximity to the rotating cylinder. The charging needles spray the electric charges by corona discharge onto the surface of the rotor while the discharging electrodes (needles) collect the charges by drawing them off the surface of the rotor.

The segments or inductors, which induce a strong electric field on the sharp edge of the ionizers. The inductor electrodes are placed behind a slightly conductive special glass cylinder. The excitation inductors lay the electric charges onto the surface of the rotor whilst the extracting inductor withdraws them. The charge collecting (ionizer) electrode and the inductor pair on the opposite side are called a pole of the machine. The inductor and the conductive glass cylinder are together called the stator. The stator, the rotor and the ionize electrodes are closed hermetically in a tank under pressure of compressed hydrogen.

2.2.2.6 Tritium Targets

Tritium solid target is especially made on copper backing. Tritium is a radioactive nuclide which decays by emission of β^- with a half life of 12.3 years. Some specifications of tritium target⁴⁰ are given below.

Activity of fresh target	: 370 GBq \pm 10%
Gross diameter of the target	: 45 mm
Active diameter of the target	: 30 mm
Thickness of the copper backing	: 1 mm

During irradiation the tritium target is cooled by a jet of cooled compressed air to reduce tritium evaporation from the hot target. Collimator diameter used was 10 mm. For the present experiment the tritium targets were imported from Radioisotope Center, POLATOM, Poland.

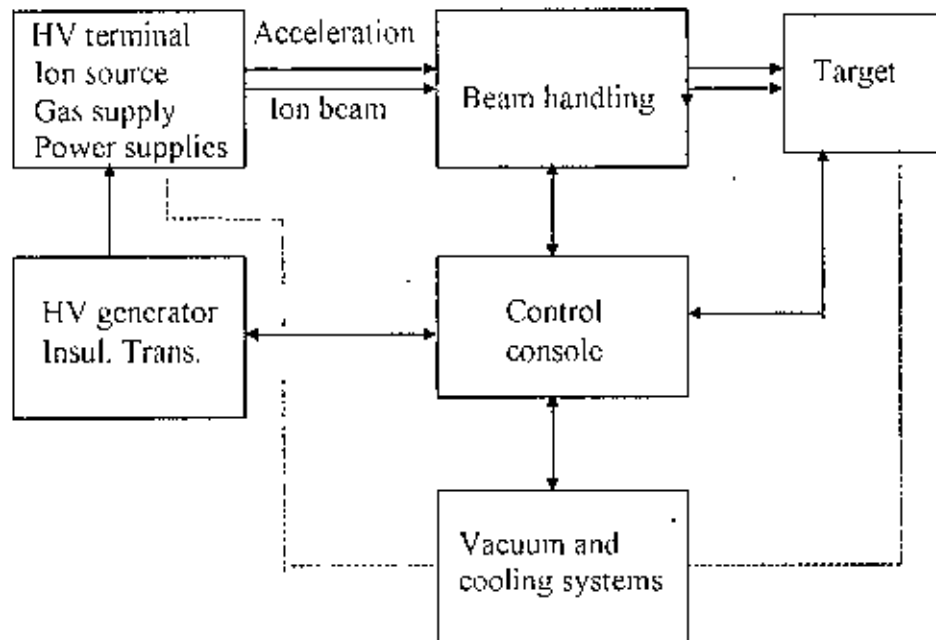
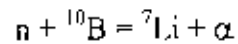


Fig.2.3. Block-diagram of neutron generator.

2.2.2.7 Neutron Monitor

The inherently low detection efficiency for fast neutrons of any slow neutron detector can be somewhat improved by surrounding the detector with a few centimeters of hydrogen-containing moderating material. The incident fast neutron can then lose a fraction of its initial kinetic energy in the moderator before reaching the detector as a lower-energy neutron, for which the detector efficiency is generally higher⁴¹. A BF_3

long counter was used inside the neutron generator room for the detection of neutrons. Paraffin was used as the moderating material. As long counter detects the neutrons by the



reaction (after thermalization), the pulses from the gamma rays associated with the neutron field can be well separated. For monitoring the neutron flux, a multichannel analyzer was used in the multiscaler mode.

CHAPTER 3
GAMMA-RAY
SPECTROMETRY SYSTEM

CHAPTER 3

GAMMA RAY SPECTROMETRY SYSTEM

The gamma-ray spectrometry system is one of the important parts in the field of instructional arrangement for measuring the reaction cross sections. It is thus essential for the experimenter to know about the different components of gamma-ray spectrometry system to assure proper function of the measuring system and assess possible sources of error in the measurement.

3.1 Interaction of Gamma rays with Matter

The interaction process of gamma rays with matter is complex. The γ photons may pass through an indefinite distance through matter without interacting i.e., without losing any energy. On the other hand, suddenly in a single encounter with atomic electron or in the nuclear field, it may lose all its energy by being captured or lose a fraction of its energy and get scattered as a photon of longer wave-length. In view of this unpredictable characteristic behavior, photons do not have a specific range in matter as the charged particles. In order to understand the detectors used for gamma-ray detection and to be able to select one for a particular measurement, it is necessary to review the ways in which gamma rays interact with matter. Although a large number of possible interaction modes are known for gamma rays with matter, only three major types play important roles in the radiation measurements are as follows.

1. Photoelectric effect
2. Compton scattering and
3. Pair production.

3.1.1 Photoelectric Effect

In photoelectric effect, the gamma ray interacts with an orbital electron, transferring all its energy to the electron and disappearing in the process as shown in Figure 3.1. The electron is ejected from the atom with a kinetic energy E_e , given by

$$E_c = E_\gamma - E_{BL}$$

where E_γ is the incoming γ -ray energy and E_{BL} is the binding energy of the ejected electron. Such a photoelectron will interact with other atoms in its path, leading to further ionization.

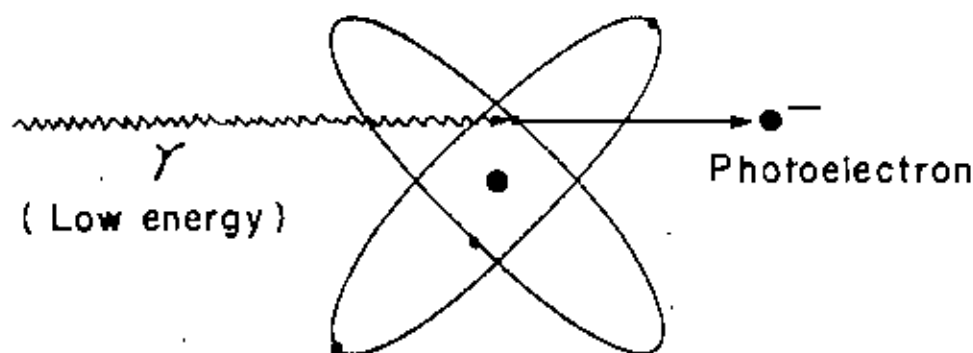


Fig. 3.1 Photoelectric effect

The photoelectric effect is most likely to happen when the γ -ray energy matches the electron binding energy, since, in the photoelectric effect, the electron must absorb all the γ -ray energy. Furthermore, the most tightly bound electrons will be most likely to absorb the γ -ray energy; that is, the photoelectric-effect probability will be greatest for K-shell electrons. No single analytic expression is valid for the probability of photoelectric absorption per atom over all ranges of Z , but a rough approximation³⁵ is

$$\tau \cong \text{constant} \times \frac{Z^n}{E_\gamma^{7/2}}$$

where Z is the atomic number of the stopping material and E_γ is the γ -ray energy. The exponent n varies between 4 and 5 over the gamma-ray energy region of interest. Thus the photoelectric effect is most important at low γ -ray energies ($0 \leq E_\gamma \leq 0.5$ MeV) and is relatively more important in heavy elements. The photoelectric effect is accompanied by X-ray emission and/or Auger electron emission. These radiations are associated with necessary rearrangements in the atomic electrons due to ejection of one electron.

3.1.2 Compton Scattering

Gamma rays of medium energy (0.5 to 1.5 MeV) may undergo elastic collisions with loosely bound orbital electrons as shown in Figure 3.2. In such cases, only a portion of the γ -ray energy is transferred to the electron, which is ejected.

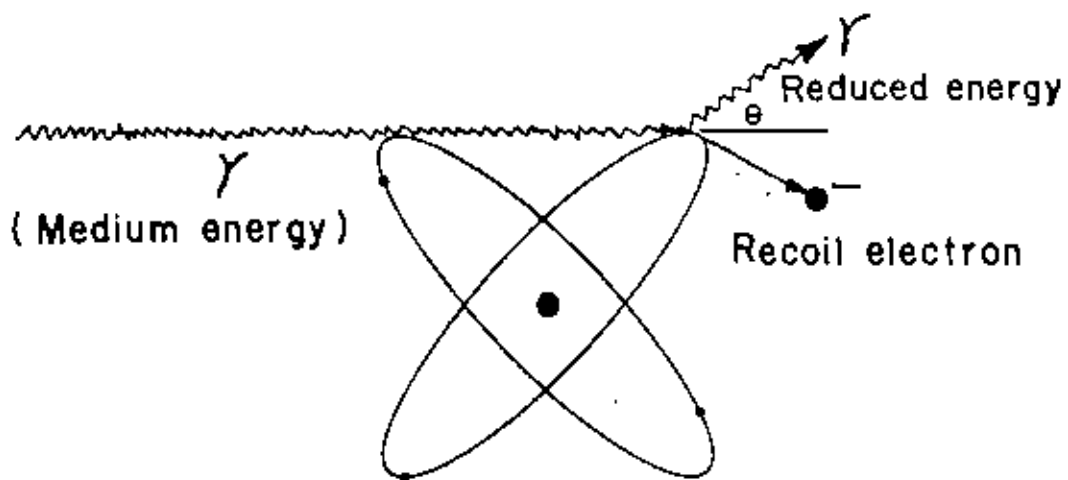


Fig. 3.2 Compton effect

The γ -ray photon itself is deflected in a new direction, with a reduced energy. These recoil electrons may carry away from such an encounter any amount of energy up to a defined maximum. The energy of electron is given by

$$E_e = hv \left[\frac{(hv/m_0c^2)(1 - \cos\theta)}{1 + (hv/m_0c^2)(1 - \cos\theta)} \right]$$

where hv = incident photon energy

m_0 = rest mass of electron

c = speed of light in vacuum

θ = angle of scattering for gamma photon

The maximum energy transfer to the electron occurs when the photon undergoes 180° back scattering, and then the electron energy $E_{e \text{ max}}$ is given by

$$E_{e \text{ max}} = \frac{E_\gamma}{1 + 0.511/2 E_\gamma}$$

where E_γ is the incident γ -ray energy in MeV. Thus Compton recoil electrons appear with a wide energy spread, although they are derived from a monoenergetic beam of incident γ -radiation. Considerable ionization can naturally be realized as these electrons dissipate their energy on interaction with matter. Moreover, the attenuated γ -ray may undergo several more such collisions before losing all its energy. The Compton effect is a favored mode of interaction for γ -rays of medium energy interacting with absorbers of medium-to-low atomic number. As in the photoelectric effect, if an inner orbital electron is ejected, X-ray and Auger electron emission will result. The probability of Compton scattering per atom of the absorber depends on the number of electrons available as scattering targets and therefore increases linearly with Z . This probability falls off gradually with increasing energy.

3.1.3 Pair Production

The third mechanism by which electromagnetic radiation can be absorbed is the production of electron-positron pair. The phenomenon of photon absorption leading

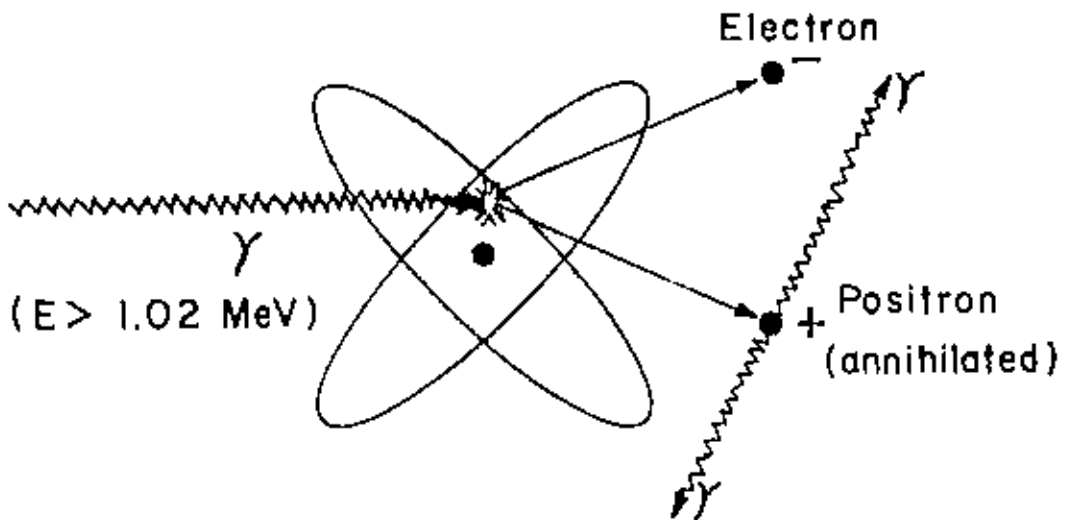


Fig 3.3 Pair production

to the creation of an electron-positron pair becomes important with photons of energies greater than 1.02 MeV. In pair production, the incident photon vanishes and a positron-electron pair is created in its place. Being an antiparticle, the positron has a short life $\sim 10^{-9}$ s and it annihilates in its turn on meeting the first electron, available all around. The $e^+ - e^-$ annihilation is accompanied⁴² by the creation of a pair of γ photons each of energy 0.512 MeV, proceeding in opposite directions as shown in Figure 3.3.

The pair production probability is given by

$$\sigma_{pp} \propto Z^2 \ln E_\gamma$$

For this to happen, the incident photon should have a minimum energy of $2m_0c^2$ (= 1.02 MeV).

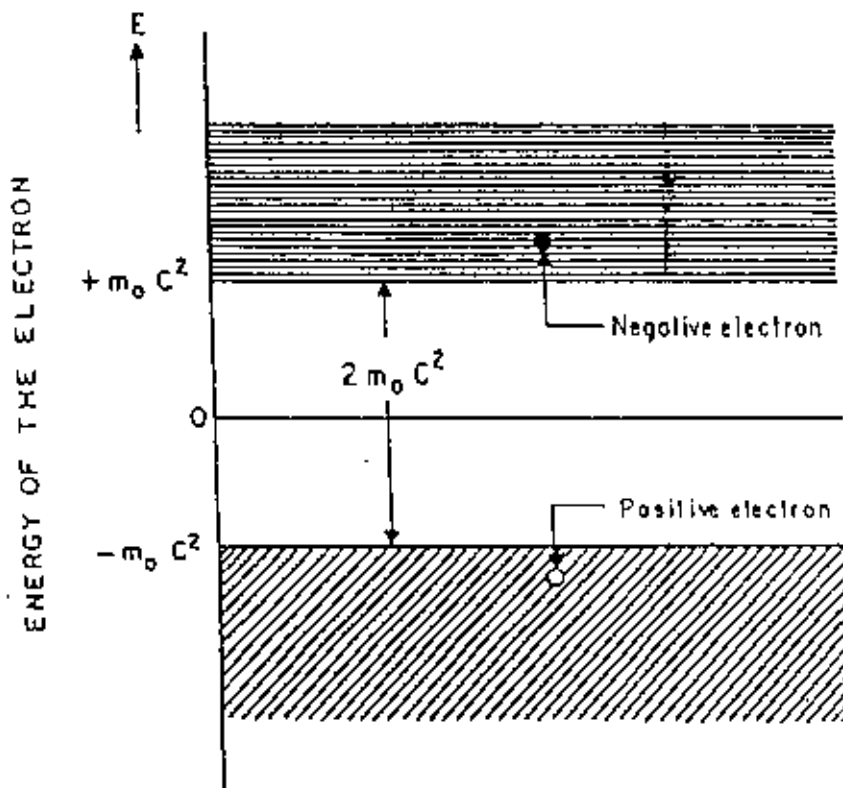
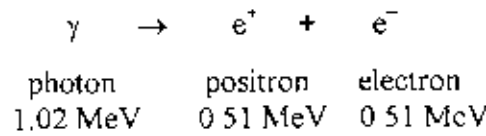


Fig. 3.4 Pair production – quantum mechanical interpretation

It was found that the possible values of the energy of a free electron are either greater than $+m_0c^2$ or smaller than $-m_0c^2$ and that no possible energies for the electron exist between these two limits. This state of affairs is shown in Figure 3.4, where the shaded regions are those in which values of the energy exist⁴³. Electrons in states of positive energy behave in the usual manner of electrons that are ordinarily observed, while electrons in states of negative energy should have properties which have no classical analogy. In terms of Dirac's theory, the production of a positron is interpreted as follows

A photon of energy greater than $2m_0c^2$ can raise an electron from a state of negative energy to a state of positive energy. The disappearance of an electron from a negative energy state leaves a hole, which means the appearance of a positron, the appearance of an electron in a positive energy state means the appearance of an ordinary electron. Thus, a pair of particles is created.

Absorption Coefficient

The probability of the interaction of γ -rays with matter can be expressed as an absorption coefficient. The resultant absorption coefficient, μ is the sum of mainly coefficients for photoelectric, Compton scattering and pair production process.

$$\mu = \mu_{pe} + \mu_{cs} + \mu_{pp}$$

Where, μ_{pe} = Absorption coefficient for photoelectric process,

μ_{cs} = Absorption coefficient for Compton scattering and

μ_{pp} = Absorption coefficient for pair production

The variation of absorption coefficients by the different modes of γ interaction with germanium^{44, 45} is shown in Figure 3.5. It has been seen that the curve for Compton effect coincides with the resultant over the region from about 0.3 to 2 MeV. The absorption of energy can be expressed per cm length of matter or per gram, atom or

electron per cm^2 in the path of the beam. The absorption coefficient depends on the energy of the incident γ -rays as well as on the nature of the absorbing material.

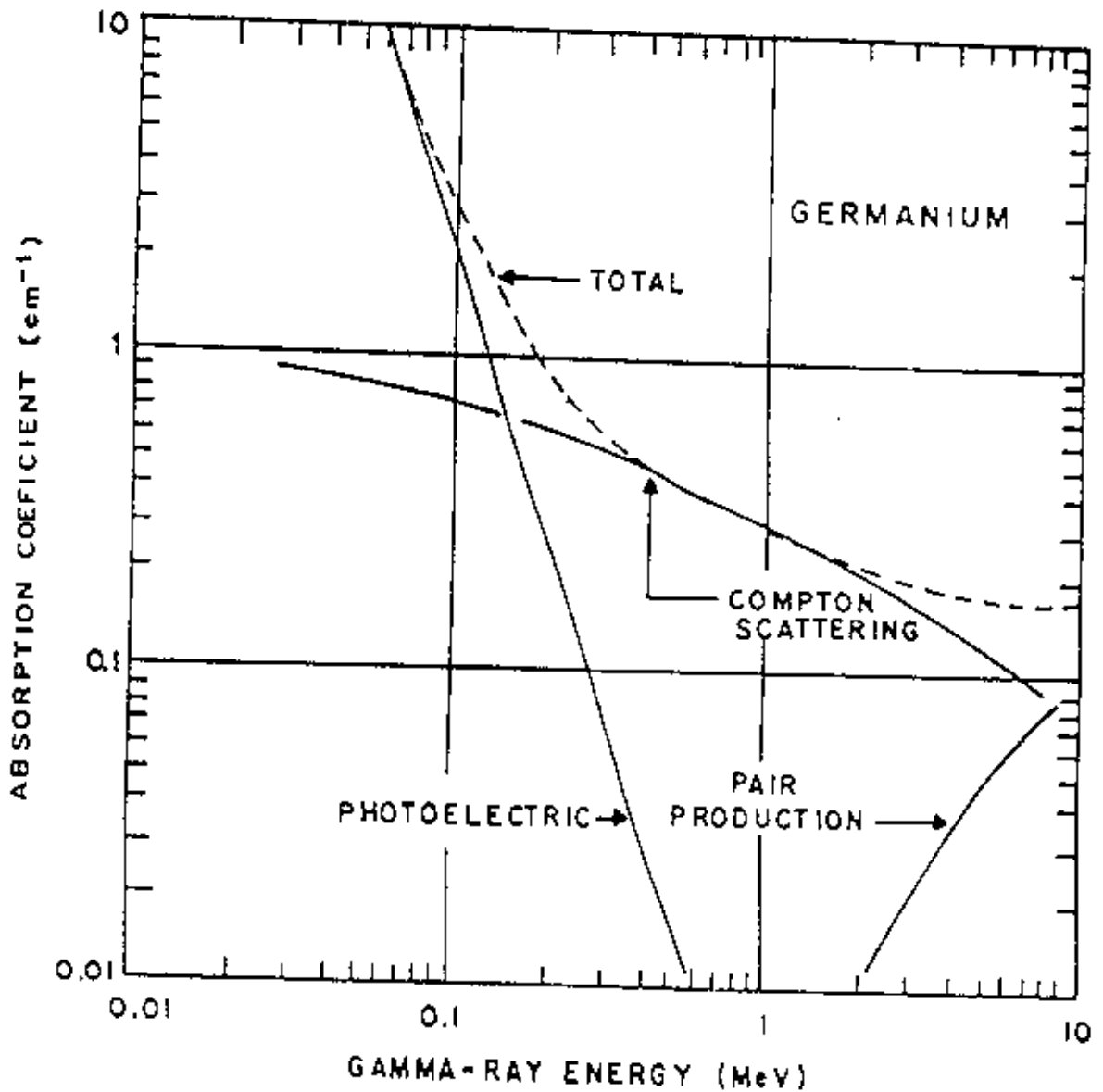


Fig. 3.5. Photon linear absorption coefficients vs photon energy for germanium.

3.2 Detection and Measurement of Gamma rays

This section provides information for the proper selection of detectors and electronics for detection and analysis of γ -ray. The choice of a particular detector type for an application depends upon the gamma energy range of interest and the application's resolution and efficiency requirements. Additional considerations

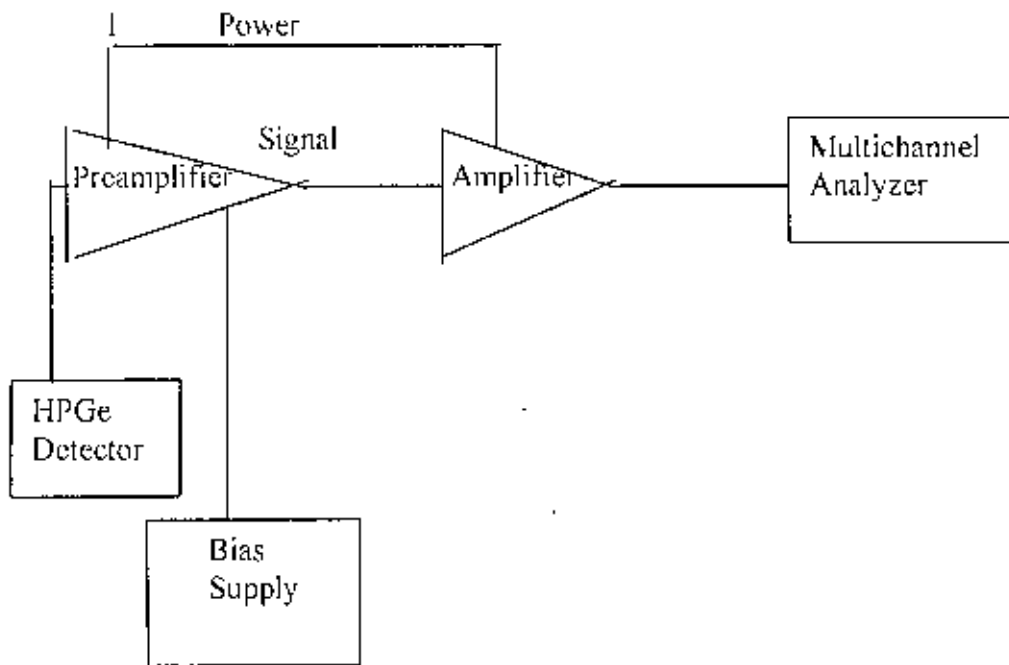


Fig 3.6 A schematic view of the electronic equipment associated with HPGe detector

include count rate performance the suitability of the detector for timing experiments and of course, price. In the present work, the detector with semiconductor material Ge has been selected. A semiconductor material is one whose electrical properties lie in between those of insulator and good conductor. Semiconductor which have almost empty conduction band and almost filled valence band with a narrow energy gap (of the order of 1 eV) separating the two. Germanium is the most frequently used semiconductor material. It is because the energy required to release an electron from their valence bands is very small¹⁶; being of 0.74 eV. In electronics the term solid state is often used interchangeably with semiconductor, but in the detector field the term can obviously be applied to solid scintillators. Therefore, semiconductor is the preferred term for those detectors which are fabricated from either element or compound single crystal materials having a band gap in the range of approximately 1 to 5 eV.



Germanium is the most widely used semiconductor. To perform the detection and counting of γ -ray, HPGe-detector associated with preamplifier, amplifier, analog-to-digital converter (ADC) and multichannel analyzer (MCA) has been used.

3.2.1 High Purity Germanium (HPGe) Detector

The conventional coaxial germanium detector is often referred to as Pure Ge, HPGe, Intrinsic Ge or Hyperpure Ge. Regardless of the superlative used, the detector is basically a cylinder of germanium with n-type contact on the outer surface and a p-type contact on the surface of an axial well. The germanium has a net impurity level of around 10^{10} atoms/cm³.

The n and p contacts or electrodes, are typically diffused lithium. The reliable performance of the detector depends on its depletion depth which is inversely proportional to the net electrical impurity concentration in the detector material and on applied potential difference. The principle in brief is that semiconductor material contains impurities which can be of the donor or the acceptor type. A donor (n-type) gives electrons to the conduction band, whereas an acceptor (p-type) takes electrons out of the valence band, thus creating a hole by forming a p-n junction. By applying a reverse biased voltage, i.e., a positive voltage to the n-type material and a negative voltage to the p-type material, electrons are "pulled farther away" from the junction and thus a depletion region is formed that is sensitive to γ -radiation. The greater the reverse bias the wider the depletion layer becomes. The depletion layer stops growing when its difference of potential equals the source voltage⁴⁷. Thus, when a γ -ray interacts within the depletion region, it causes ionization and creates holes in the valence band and electrons in the conduction band^{48,49}. The electrons migrate to the positive voltage on the n-side, while the holes migrate to the negative voltage on the p-side, thereby creating an electrical output signal which is directly proportional to the amount of incident γ -ray energy absorbed in the depletion region. In a Ge(Li) detector only 2.9 eV needed to obtain the equivalent of one ion pair. As a practical matter Ge detector must be cooled in order to prevent rediffusion of the Li and to reduce the thermal charge carrier generation (noise).

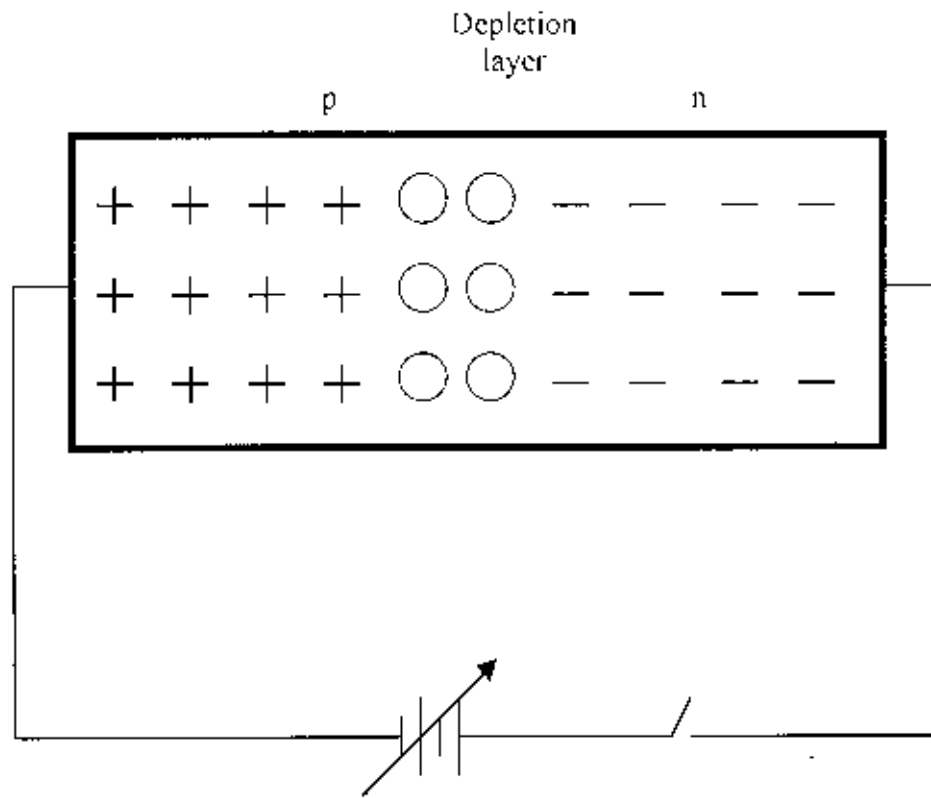


Fig. 3.7 Formation of depletion layer across a p-n junction

to an acceptable level. The most common medium for detector cooling is liquid nitrogen. In liquid nitrogen (LN_2) cooled detectors, the detector element (and in some cases preamplifier components), are housed in a clean vacuum chamber which is attached to or inserted in a LN_2 Dewar. The detector is in thermal contact with the liquid nitrogen which cools it to around 77°K or -196°C . At these temperatures, reverse leakage currents are in the range of 10^{-9} to 10^{-12} amperes.

HPGe detectors provide greatly improved energy resolution over other types of radiation detectors for many reasons. Fundamentally, the resolution advantage can be attributed to the small amount of energy required to produce a charge carrier and the consequent large output signal relative to other detector types for the same incident photon energy. A cross-sectional view of a coaxial germanium detector is shown in Figure 3.8. Some important dimensions of the closed end vertical dipstick detector are mentioned below.

Diameter	: 4.1 cm
Length	: 5.5 cm
Active area facing the window	: 17.50 cm ²
Distance from the window	0.5 cm

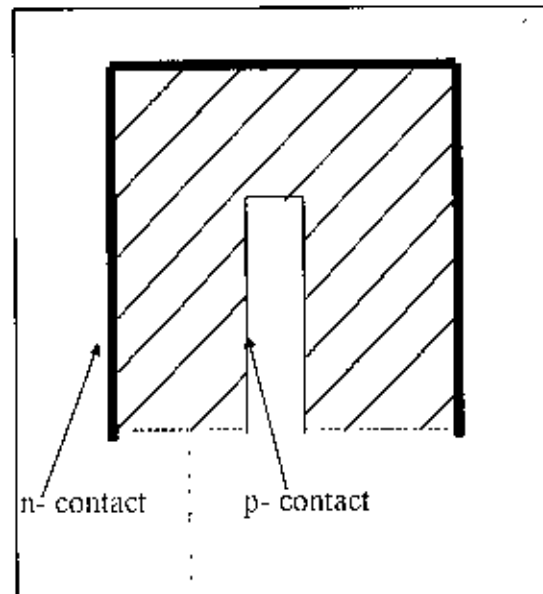


Fig. 3.8 Coaxial germanium detector cross section⁵⁰. The hatched region indicates active volume for gamma ray interaction

3.2.2 High Voltage Power Supply

An external high voltage called “detector bias” is used for operation and optimum performance of radiation detectors. The high voltage module is a d.c. converter where low voltage d.c output which is regulated, filtered and can be varied by the front panel controls. The unit is powered from a standard Nuclear Instrumentation Modules (NIM) bin power supply.

The Canberra model 3105 is suitable for use with high resolution detector systems. It is a NIM high voltage power supply, designed primarily for operation with semiconductor detectors and can accommodate all types of detectors requiring up to 5 kV bias with a current of 100 μ A. The applied bias voltage to the detector used in our experiment was

4,000 volts. The 3105 Canberra power supply can withstand any overload or direct output short circuit for an infinite period of time and provide normal output when the ONN-OFF switch is reset. Output voltage can be continuously adjusted over the full range, 0 to $\pm 5,000$ volts by means of five turn control.

3.2.3 Preamplifier

The preamplifier associated with radiation detectors performs four essential functions:

- i) Conversion of charge to voltage pulse
- ii) Signal amplification
- iii) Pulse shaping
- iv) Impedance matching

Most preamplifiers in use today are charge sensitive and provide an output pulse with an amplitude proportional to the integrated charge output from the detector. General purpose preamplifiers have a RC feedback network which results in a quasi-step function output.

The preamplifier is isolated from the high voltage by a capacitor. The rise time of the preamplifier's output pulse is related to the collection time of the charge, while decay time of the preamplifier's output pulse is the RC time constant characteristic of the preamplifier itself. Rise times range from a few nanoseconds to a few microseconds, while decay times are usually set at about 50 microseconds. The RC preamplifier gives better performance at high total energy rates. It is, therefore, used exclusively on larger detectors which have greater stopping power for high energy photons.

To maximum performance, the preamplifier should be located at the detector to reduce capacitance of the leads, which can degrade the rise time as well as lower the effective signal size. Additionally, the preamplifier also serves to provide a match between the impedance of the detector and the low impedance of coaxial cables to the amplifier, which may be located at great distances from the preamplifier. Canberra model-2001 is an advanced type of charge sensitive preamplifier which has been used in the present work. A few major characteristics of the preamplifier are as follows:

1. The pulse time is less than 40 n sec
2. The pulse decays exponentially with a time constant of 50 μ sec
3. The source capacity is 0 pF
4. The noise level is equivalent to less than 600 eV

3.2.4 Amplifier

The major role of an amplifier is to convert the preamplifier output signal into a form most suitable for the measurement desired. Since the number of applications and signal characteristics are numerous, so are there many techniques for treating the signal to optimize each application. The amplifier serves to shape the pulse as well as further amplify it. The purpose of this additional amplification and shaping is two fold. First, further amplification improves the signal-to-cable noise ratio. Secondly, further shaping acts to prevent pulse overlap by clipping pulses. The spectroscopy amplifier provides a uni-polar output and include pole zero cancellation and rapid baseline restoration after the occurrence of a pulse. The important characteristics of the amplifier are the linearity, the output pulse shape, the gain stability and the noise level. Canberra model-2022 amplifier is used in this experiment. It offers the better resolution performance features and flexibility than any other nuclear pulse amplifier used commercially.

3.2.5 Multichannel Pulse Height Analyzer

The heart of the multichannel analyzer is the analog-to-digital converter (ADC), which converts the incoming analog amplifier signal to a group of standard-shaped pulses. If the incoming pulse is 4 volts, the ADC might produce 400 standard pulses; or if the incoming pulse was 3 volts, 300 pulses would be produced. In this way, analog information (the signal height) is converted to digital information (the number of pulses).

The most commonly used ADC design is that of Wilkinson. First, the input signal is given flat-top, using a pulse-stretching network. When the input signal reaches its peak amplitude, an oscillator is turned on, thereby producing a train of standard pulses, and a

linearly rising voltage is also turned on. When the voltage of the input signal and the linearly rising signal become equal, the oscillator is turned off. Consequently, the bigger the initial signal voltage, the longer it will take for the linearly rising voltage to equal the input signal amplitude and the oscillator will produce more pulses. The pulses from the ADC are counted by the address scaler, and the resultant number is said to be the address (channel number) of that signal. At each memory location or channel, a counter records the number of occurrences of the incoming signal.

For the present experiment PC based System 100 MCA boards and software were used for data acquisition and display. The System 100 MCA has a full 16K channels of data memory, which can be configured as 4K (4096 channels), 8K (8192 channels), or the entire 16K (16384 channels). Some features of S 100 MCA are

- Vertical axis in linear or log scale
- Built-in energy calibration function
- Built-in peak analysis function
- Built-in live time correction function
- Read out of dead time in percentage

3.3. Energy Calibration of the MCA

The S 100 MCA has a built-in energy calibration function which calibrates each channel in the displayed spectrum for a specific energy unit. It allows unknown peaks to be identified by their locations in the calibrated spectrum.

Least square method is applied for first or second order fitting but first order (straight line) fitting is sufficient for most of the cases. Channel number is assigned as independent variable while energy (keV) is assigned as dependent variable.

Table 3.1 List of standard calibrated sources with gamma-ray energy

Radioactive source	Half life	Gamma-ray energy (keV)
²² Na	2.6y	511
⁵⁷ Co	271.76d	122.06
		136.48
⁶⁰ Co	5.27y	1173.23
		1332.51
¹³³ Ba	10.54y	80.99
		276.40
		302.85
		356.01
¹³⁷ Cs	30.14y	383.85
		661.64

Then relationship between keV and channel numbers is established as

$$\text{keV} = m \times \text{channel number} + C \quad (1)$$

where, slope m (keV/channel) and C (intercept from the energy axis) are two unknown coefficients which must be determined by least square fitting method. To determine these two coefficients a spectrum was acquired using the standard calibrated sources listed in Table 3.1.

From the spectrum 12 pairs of energies (keV) and channel numbers were obtained and these were used as input data pairs for the least square fitting. The results of the fitting were

$$\text{keV/channel} = 0.603466$$

$$\text{Intercept from the energy axis} = 1.30222 \text{ keV}$$

Now equation (1) becomes

$$\text{keV} = 0.603466 \times \text{channel number} + 1.30222 \quad (2)$$

With the help of relationship (2) keV corresponding to a particular channel number can be directly read out.

3.4 Measurements of Detector Parameters

3.4.1 Energy Resolution

Energy resolution of a detector or spectroscopy system is a measure of its ability to differentiate between two peaks that are close together in energy. Thus the narrower the peak, the better the resolution capability. It is specified in terms of full width at half maximum (FWHM) for 1332.51 keV peak of ^{60}Co . Resolution is a function of gamma-ray energy.

The overall energy resolution achieved in a germanium system is normally determined by a combination of three factors, the inherent statistical spread in the number of charge carriers, variation in the charge collection efficiency, and contributions of electronic noise⁴¹

To measure the resolution of the HPGe detector a spectrum was acquired using ^{60}Co source for a counting time of 600 sec. In ^{60}Co spectrum there are two gamma-ray peaks, one is at 1173.23 keV and another is at 1332.51 as shown in Table 3.1. The peaks are 159.28 keV apart. For the region of the two peaks experimental data were plotted by putting channel numbers in X-axis and counts in Y-axis. From the graph, the full width at half maximum (FWHM) value was found to be 3.4 channels at 1332.51 keV peak. Resolution in keV can be determined from the following relationship

$$\text{Resolution} = \text{FWHM (channels)} \times \frac{159.28 \text{ keV}}{\text{No. of channels between the peaks}}$$

The detector resolution (FWHM) obtained in this measurement was 1.94 keV at 1332.51 keV peak of ^{60}Co

The dominant characteristics of germanium detectors is their excellent energy resolution when applied to gamma-ray spectrometry. The great superiority of the germanium system in energy resolution allows the separation of many closely spaced gamma-ray energies, which remain unresolved in the NaI (TI) spectrum. A narrow peak includes fewer channels and fewer background counts. So, accuracy of measurement increases when high-resolution measuring system is used.

3.4.2 Efficiency Measurement

Efficiency of a detector relates the number of detector pulses to the number of gamma rays emitted by the source. It allows us to convert the count obtained from spectral analysis to unit of activity. Efficiency changes with the physical change of the counting system.

Using standard calibrated sources listed in Table 3.1, spectra were acquired at 8 cm above the surface of the detector for a counting time sufficient for peak area equal to or greater than 10,000. Counts were taken at a distance from the surface of the detector to avoid coincidence losses when a single source emits more than one gamma-ray energy. ^{137}Cs has single energy, hence spectra for ^{137}Cs were acquired both at 8 cm and at the surface. The ratio of the counts at surface of the detector to the counts at 8 cm from the surface of the detector for ^{137}Cs with the same counting time is called the normalizing factor by which counts of the all other sources are multiplied to obtain counts at the surface of the detector. Efficiency at the surface of the detector can be determined from the following relationship

$$\text{Efficiency} = \frac{\text{Detected count / sec}}{\text{Present activity of the source} \times I_\gamma}$$

where I_γ is the number of gamma rays per disintegration,

$$\text{Detected counts / sec} = \frac{\text{Net area under a photopeak}}{\text{Counting time (Sec)}}$$

Present activity of the source is given by

$$A_t = A_0 e^{-\lambda t}$$

where A_t = present activity of the source,

A_0 = Initial activity of the source,

t = Decay time,

λ = Decay constant

The efficiency for a particular gamma ray depends on detector size, shape and types of material, especially the atomic number of the material, source-detector distance and experimental geometry. The measured efficiencies as a function of gamma-ray energy are plotted in Figure 3.9.

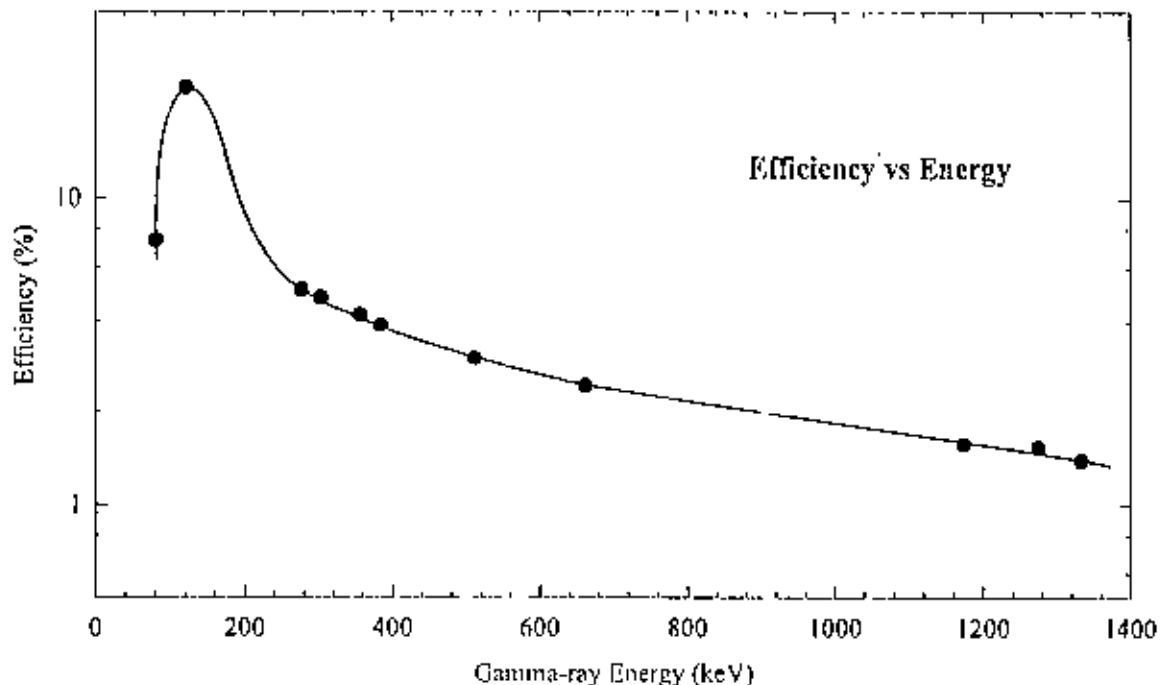


Fig. 3.9 Detector efficiency as a function of gamma-ray energy

3.4.3 Background Radiation

For the present work, the background effect is very important in detecting gamma rays by high purity germanium (HPGe) detector. Some counts in the detector were observed due to background radiation during the experiment. These counts are mainly produced by the cosmic radiation because of its interaction with earth's atmosphere and it determines the minimum detectable radiation level. The background counts depend

upon the size and type of the detector and also upon the shielding around it. The sources of background radiation are as follows.

Radioactivity in the air surrounding the detector

1. Radioactivity from the earth's surface (the terrestrial radiation), walls of the laboratory or other far away structures.
3. Natural radioactivity of the constituent materials of the detector itself
4. Some fission products activities
5. Activity of cosmic ray that continuously interacts with earth's atmosphere.

3.4.4 Shielding Arrangement of the Detector

For the protection of background of the detector, shielding arrangement is very essential. The shielding not only reduces the background resulting from cosmic radiation and from natural radioactive traces in the building materials or in the surface of the earth, but also from nearby nuclear facilities and other radiation sources like air, which presumably contains trace of radioactive gases, Radon (Rn) and Thorium (Th 220) etc.

Mathematically the shielding effectiveness is expressed as

$$I = I_0 e^{-\mu x}$$

where I_0 is the initial beam intensity, I is the beam intensity after penetrating a thickness t of the material and μ is the linear absorption coefficient of the material of the shield

In our experiment, lead is used as shielding material across the HPGe detector. The important advantages of lead are high density (11.4 g / cc), large atomic number ($Z=82$) and comparatively low cost. A brief description of the shielding used in the experiment is summarized in the Table 3.2

Table 3.2 Summary of shielding arrangement around the HPGe Detector

	Material	Lead
	Length	14.5 cm
Low background shielding	Height	12.5 cm
	Thickness	4 cm
	Form	Square

CHAPTER 4
MEASUREMENT OF (n,2n), (n,p) AND
(n, α) REACTION CROSS SECTIONS ON
THE ISOTOPES OF Mo, Co, Zr AND Ge
IN THE NEUTRON ENERGY RANGE
13.90 – 14.80 MeV

CHAPTER 4

**MEASUREMENT OF (n,2n), (n,p) AND (n,α) REACTION CROSS SECTIONS
FOR ISOTOPES OF Mo, Co, Zr and Ge IN THE NEUTRON ENERGY RANGE
13.90 - 14.80 MeV**

In order to determine the most precise and reliable cross section data for the reactions $^{92}\text{Mo}(n,p)^{92m}\text{Nb}$, $^{94}\text{Mo}(n,2n)^{93m}\text{Mo}$, $^{96}\text{Mo}(n,p)^{96}\text{Nb}$, $^{59}\text{Co}(n,\alpha)^{56}\text{Mn}$, $^{90}\text{Zr}(n,2n)^{89}\text{Zr}$, $^{70}\text{Ge}(n,2n)^{69}\text{Ge}$, $^{74}\text{Ge}(n,\alpha)^{71m}\text{Zn}$ and $^{76}\text{Ge}(n,2n)^{75m}\text{Ge}$ in the energy range of 13.90 to 14.80 MeV, precision measurements were carried out by the activation technique in combination with high resolution HPGe detector gamma-ray spectrometry. For convenience the reactions are arranged in two groups and discussed in the subsequent sections.

4.1 Measurement of Cross Sections for Molybdenum and Cobalt Isotopes:

Experimental Procedure

In the present experiment, high purity target materials of molybdenum trioxide powder of natural isotopic composition and cobalt foil were used. One molybdenum sample was prepared in the form of pellets by applying pressure of 7 tons using a hydraulic press. This pellet has the diameter 1.2 cm and thickness ~0.15 cm. Mass of these pellet was between 0.7295g and 0.8519g. The molybdenum pellet was then sealed in thin polyethylene bag. One cobalt foil was made round shaped and cleaned well by acetone. Mass of this foil was 0.1527g. Molybdenum pellet and cobalt foil was sandwiched between aluminium flux monitor foils of same diameter as it. Mass of the each aluminium foil was between 0.1916 and 0.2035 g. The samples were sandwiched between flux monitor foils. Then the samples and the aluminium foils were irradiated at the neutron generator facility of the Institute of Nuclear Science and Technology (INST), Atomic Energy Research Establishment, Savar, Dhaka. The Neutron generator operation data are as follows

Beam current . 120 μA

Beam diameter . 10 mm

Deuteron energy : 110 keV

Irradiation time : 1.5 hours

During the irradiation, the target was cooled by a jet of cold air. A BF_3 long counter was placed at 2 m from the tritium target and at 45° relative to the incoming deuteron beam and was used with MCA series 40 for monitoring the relative change of neutron flux. The MCA series 40 was used in multichannel scaler mode to record neutron counts every ten seconds.

After the irradiation, induced activities in the samples and the flux monitor foils were determined by measuring the gamma-ray counts with high resolution HPGe detector gamma-ray spectrometry. Counting of the samples and the flux monitor foils were performed under the same geometry as was used at the time of efficiency measurement of the detector. Using the measured count rates, efficiency of the detector and other decay data, activities at the end of irradiation were determined by the following equation

$$DPS = \frac{CPS}{\epsilon \times I_\gamma} e^{\lambda t_d}$$

The cross section values of the desired reactions were calculated using the following standard activation equation

$$\sigma = \frac{DPS}{N\phi(1 - e^{-\lambda t_i})}$$

where, CPS = Net area under a photo-peak / counting time

I_γ = Gamma-ray intensity of the source.

t_d = Decay time

ϵ = Efficiency of the detector

N = Total number of target nuclei

$$= \frac{W \times F \times N_A}{M}$$

M = Atomic weight

F = Isotopic abundance of target nuclei

W = Weight of sample in gram.

N_A = Avogadro's number (6.023×10^{23} atoms/mole)

ϕ = Neutron flux ($n \text{ cm}^{-2} \text{ sec}^{-1}$).

t_i = Irradiation time (sec).

σ = Cross section (mb).

DPS= Disintegration per second

λ = Decay constant $= 0.693/T_{1/2}$

$T_{1/2}$ = Half-lives of the product radionuclide

Energy of the neutron as a function of emission angle was determined earlier¹⁹ in this laboratory by measuring the ratio of ⁸⁹Zr to ^{92m}Nb specific activities produced in Zr and Nb foils by (n,2n) reaction at different angular positions. The energy of neutron for the sample position is shown in the 3rd column of Table 4.1.

The neutron flux at each sample position was determined using ²⁷Al(n,α)²⁴Na monitor reaction. For the determination of flux, cross sections of the monitor reaction at different energies were taken as input from the works of H. Vonach⁵¹⁷. These cross sections are shown in the 4th column of Table 4.1. To determine neutron flux, the following equation was used

$$\phi = \frac{DPS}{N\sigma(1 - e^{-\lambda t_i})}$$

The description of the notations used in above equation are mentioned in previous equation. Neutron energy and flux at surface of tritium target are shown in the 3rd and 5th columns of Table 4.1 respectively. The decay data for the reactions were taken from the literature^{13, 52} and shown in Table 4.3.

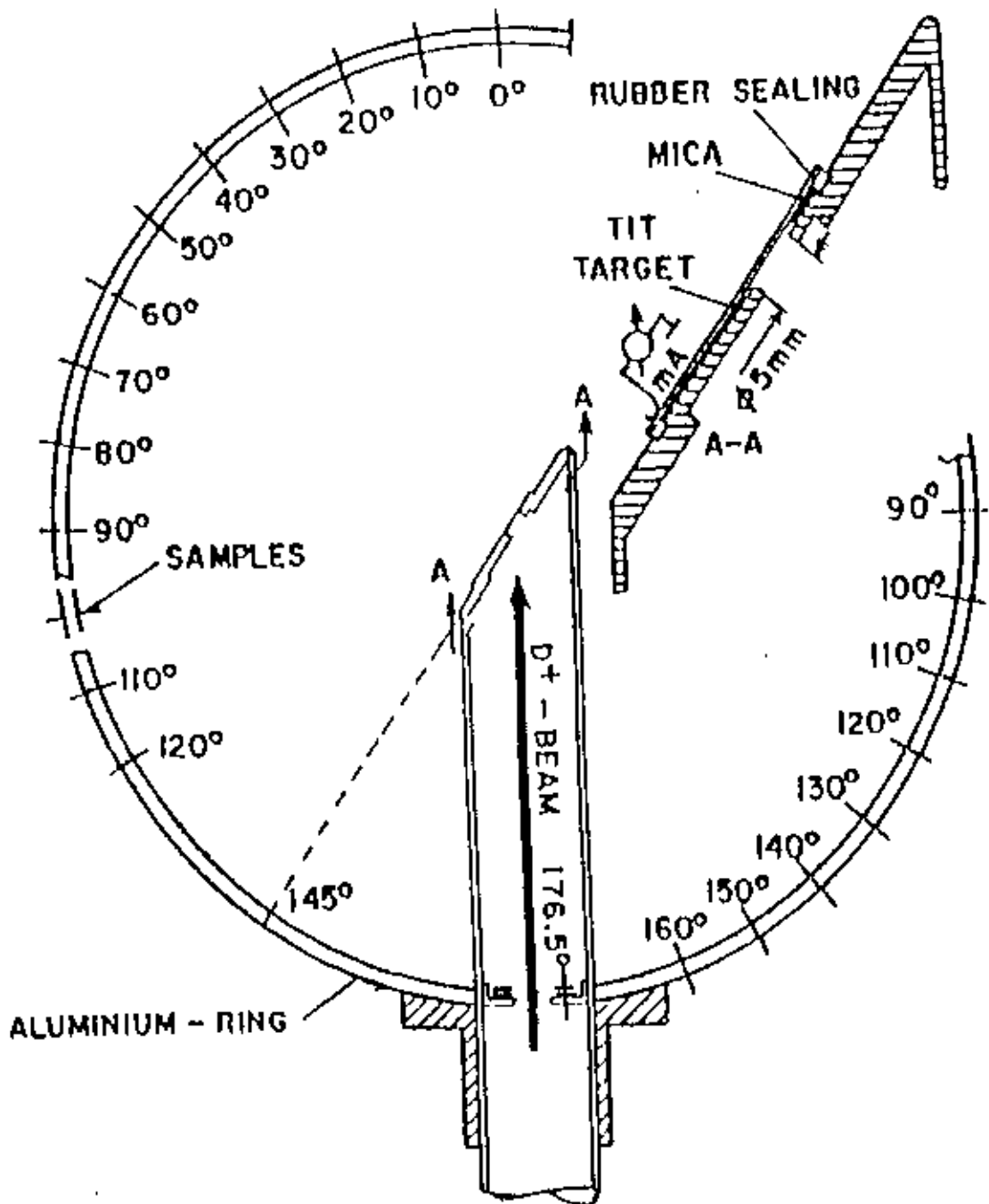


Fig. 4 1. A sketch of the scattering-free ring geometry arrangement for the irradiation of samples

Table 4 1 Neutron energy and flux at surface of tritium target for the molybdenum and cobalt samples

Sample position	Sample	Energy of neutron (MeV)	Cross-section of $^{27}\text{Al}(n,\alpha)^{24}\text{Na}$ reaction (mb)	Neutron flux $\text{n/cm}^2/\text{s} \times 10^6$
Surface	Mo	14.80	113.10	5.76
Surface	Co	14.80	113.10	5.24

Partial decay schemes of the product nuclei and the origin of the gamma rays measured are shown in Figures 4.2-4.8⁵³. The decay data for the reactions were taken from the literature^{25, 52} and are shown in Table 4.3. Measured cross section values are shown in Table 4.4. For all the cross section values two to three independent measurements were carried out and both the statistical and systematic errors were considered to evaluate total error. Table 4.5 shows the principal sources of systematic errors.

4.2 Measurement of Cross Sections for Germanium and Zirconium Isotopes: Experimental Procedure

Germanium from E. MERCK, Germany, in powder form was used to make four pellets by applying a pressure of 6 tons using a hydraulic press. Mass of the each pellet was between 0.4971 and 0.7142 g. The germanium pellets were then sealed in thin polyethylene bags and sandwiched by 2 aluminium (purity 99%) flux monitor foils. Mass of the each aluminium foil was between 0.1852 and 0.2067 g. Extremely pure zirconium (purity 99.5%) foils were made square shaped and cleaned well by acetone. Mass of the each foil was between 0.1458 and 0.1558 g. Each zirconium foil was sandwiched by 2 aluminium flux monitor foils. Mass of the each aluminium foil was between 0.1739 and 0.1972 g. The scattering-free ring geometry arrangement shown in Fig. 4.1 was used for the irradiation of the samples and the flux monitor foils at 6.6 cm from the D-1 source. The samples and the monitor foils were fastened to the ring which was accurately graduated for the indication of angular positions. The angular positions of the samples with respect to the direction of deuteron beam were 10° , 40° , 70° and 110° for germanium and 0° , 20° , 60° and 90° for zirconium. Then the samples and the aluminium foils were irradiated at the neutron generator facility of the Institute of Nuclear Science and Technology (INST), Atomic Energy Research Establishment, Savar, Dhaka. In the present experiment, the main operational parameters of the neutron generator are as follows

Deuteron energy	: 110 keV
Beam current	: ~130 μ A
Beam diameter	: ~1 cm
Irradiation time	: 3.5 hours

Neutron energy and flux at different sample positions were determined by the procedure described in section 4.1 and shown in the 3rd and 5th columns of Table 4.2 respectively

Table 4.2 Neutron energy and flux at different angular positions for the zirconium and germanium samples

Sample position	Sample	Energy of neutron (MeV)	Cross section of $^{27}\text{Al}(n,\alpha)^{24}\text{Na}$ reaction (mb)	Neutron flux $n/\text{cm}^2/\text{s} \times 10^5$
0°	Zr-1	14.71 ± 0.115	113.10	9.45
10°	Ge-1	14.70 ± 0.113	113.10	9.02
20°	Zr-2	14.63 ± 0.111	113.10	9.13
40°	Ge-2	14.51 ± 0.108	114.52	9.04
60°	Zr-3	14.31 ± 0.086	117.54	8.26
70°	Ge-3	14.21 ± 0.075	119.87	8.01
90°	Zr-4	14.00 ± 0.040	121.91	7.95
110°	Ge-4	13.90 ± 0.060	123.05	7.70

Table 4.3 Nuclear and other related data concerned in this work^{25, 54, 55}

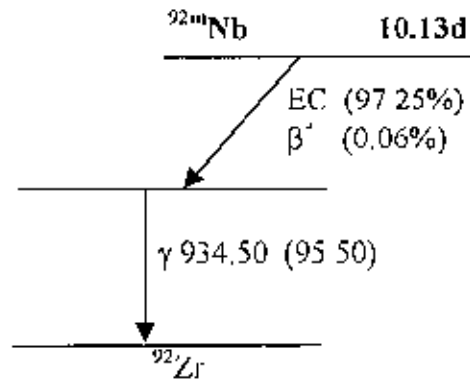
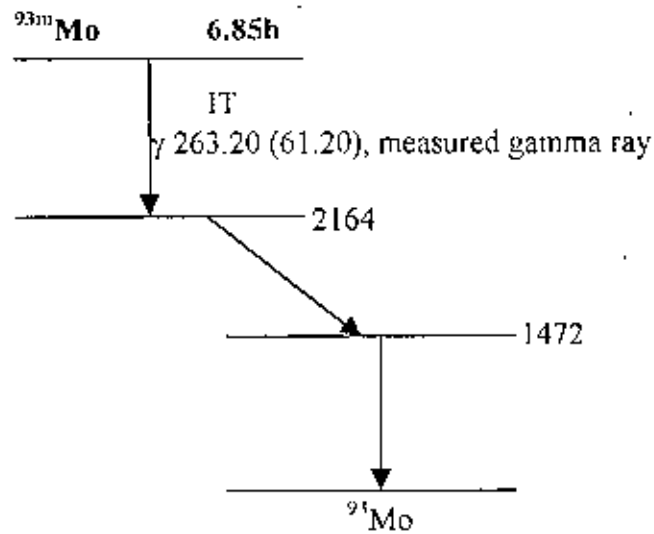
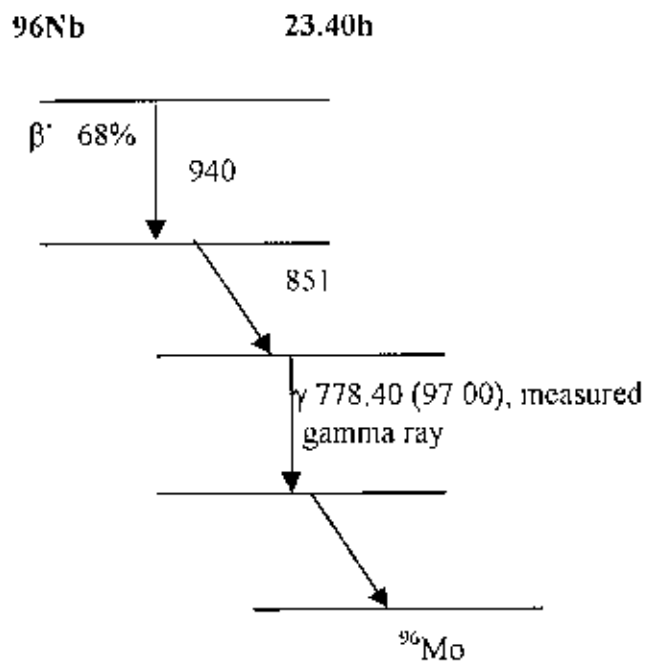
Target nucleus	Reaction	Product nucleus	Half-life	Gamma-ray energy (keV)	Gamma-ray intensity, I_γ (%)
^{27}Al	(n, α)	^{24}Na	14.96 h	1368.6	100
^{92}Mo	(n, p)	$^{92\text{m}}\text{Mo}$	10.13 h	934.50	95.50
^{94}Mo	(n, 2n)	$^{93\text{m}}\text{Mo}$	6.85 h	263.20	61.20
^{96}Mo	(n, p)	^{96}Nb	23.40	778.40	97.00
^{59}Co	(n, α)	^{56}Mn	2.582 h	846.60	99.00
^{90}Zr	(n, 2n)	^{89}Zr	3.27 d	909.10	99.00
^{70}Ge	(n, 2n)	^{69}Ge	39.2 h	511.00	28.40
^{74}Ge	(n, α)	$^{71\text{m}}\text{Zn}$	3.97 h	386.30	93.00
^{76}Ge	(n, 2n)	$^{75\text{m}}\text{Ge}$	82.8 m	264.80	12.00

Table 4.4 The (n,2n), (n,p) and (n, α) reaction cross sections for isotopes of Mo, Co, Zr and Ge in the neutron energy range 13.90 - 14.80 MeV

Nuclear reaction	Neutron energy (MeV)	Measured reaction cross section (mb)
$^{92}\text{Mo}(n,p)^{92m}\text{Nb}$	14.80	58.37 \pm 4.6
$^{94}\text{Mo}(n,2n)^{93m}\text{Mo}$	14.80	6.95 \pm 1.01
$^{96}\text{Mo}(n,p)^{96}\text{Nb}$	14.80	25.06 \pm 0.07
$^{59}\text{Co}(n,\alpha)^{56}\text{Mn}$	14.80	31.8264 \pm 1.3428
$^{90}\text{Zr}(n,2n)^{89}\text{Zr}$	14.71 \pm 0.11	814.35 \pm 70.62
	14.69 \pm 0.11	710.20 \pm 53.73
	14.41 \pm 0.08	750.07 \pm 51.67
	14.10 \pm 0.04	638.86 \pm 42.53
$^{70}\text{Ge}(n,2n)^{69}\text{Ge}$	14.70 \pm 0.11	449.25 \pm 32.63
	14.57 \pm 0.10	435.27 \pm 32.21
	14.31 \pm 0.07	417.03 \pm 35.82
	13.90 \pm 0.06	405.98 \pm 33.57
$^{74}\text{Ge}(n,\alpha)^{71m}\text{Zn}$	14.70 \pm 0.11	3.75 \pm 0.27
	14.57 \pm 0.10	3.29 \pm 0.25
	14.31 \pm 0.07	3.24 \pm 0.30
	13.90 \pm 0.06	2.97 \pm 0.17
$^{76}\text{Ge}(n,2n)^{75m\beta}\text{Ge}$	14.70 \pm 0.11	1203.24 \pm 98.08
	14.57 \pm 0.10	1179.35 \pm 95.21
	14.31 \pm 0.07	1182.55 \pm 46.13
	13.90 \pm 0.06	1127.62 \pm 44.07

Table 4.5 Principal sources of uncertainty and their magnitude

Sources of uncertainty	Magnitude (%)
1. Irradiation geometry	0.5-1.5
2. Sample weight	0.2
3. Statistics of counting	0.5 - 7.0
4. Efficiency of the detector	1.5 - 3.0
5. Error in flux determination	1.0 - 2.0
6. Neutron absorption and scattering within the samples	0.5
7. Self absorption of gamma ray in sample	0.5
8. Gamma-ray emission probability	0.3 - 1
9. Decay data	0.2 - 1
10. Neutron flux variation with time	0.5 - 1.5

Fig. 4.1. Partial decay scheme of the product nucleus of $^{92}\text{Mo}(n,p)^{92m}\text{Nb}$ reactionFig. 4.2. Partial decay scheme of the product nucleus of $^{94}\text{Mo}(n,2n)^{93m}\text{Mo}$ reaction.Fig. 4.3. Partial decay scheme of the product nucleus of $^{96}\text{Mo}(n,p)^{96}\text{Nb}$ reaction.

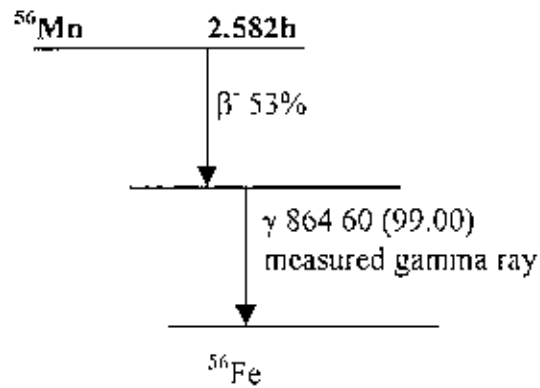


Fig. 4.4 Partial decay scheme of the product nucleus of $^{59}\text{Co}(n,\alpha)^{56}\text{Mn}$ reaction.

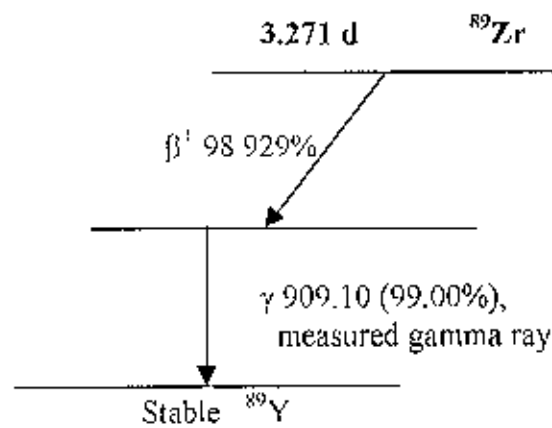


Fig. 4.5 Partial decay scheme of the product nucleus of $^{90}\text{Zr}(n,2n)^{89}\text{Zr}$ reaction.

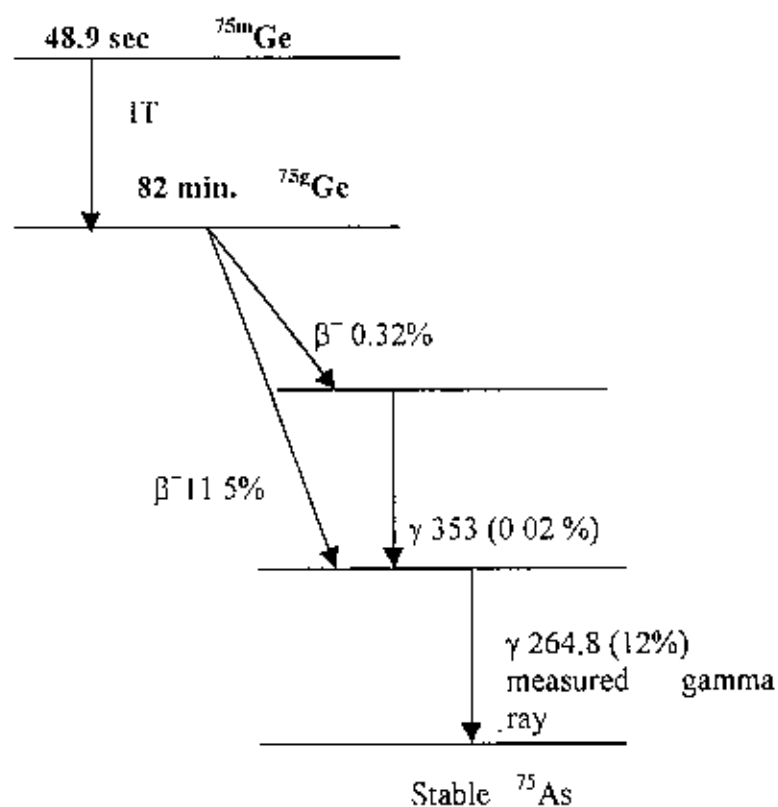


Fig. 4.6 Partial decay scheme of the product nucleus of $^{76}\text{Ge}(n,2n)^{75m}\text{Ge}$ reaction.

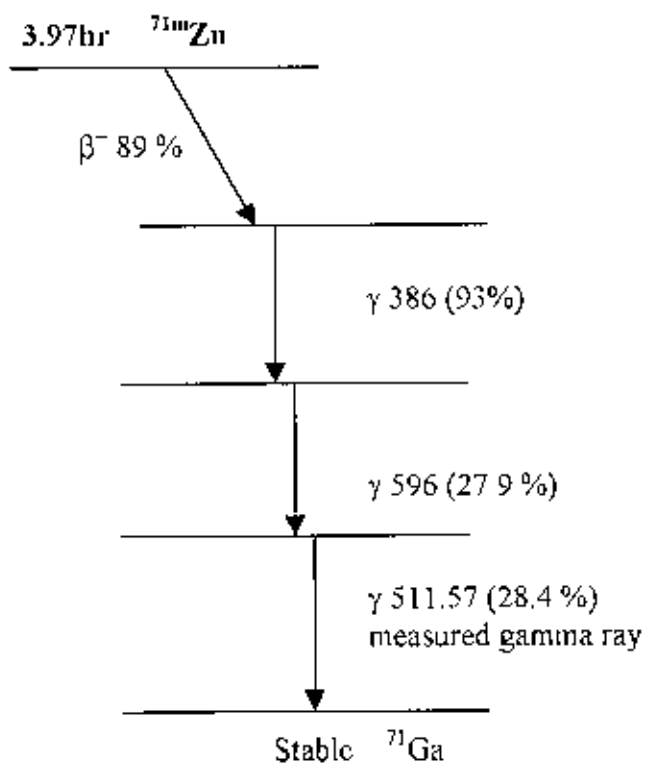


Fig. 4.7. Partial decay scheme of the product nucleus of $^{74}\text{Ge}(n,\alpha)^{71m}\text{Zn}$ reaction

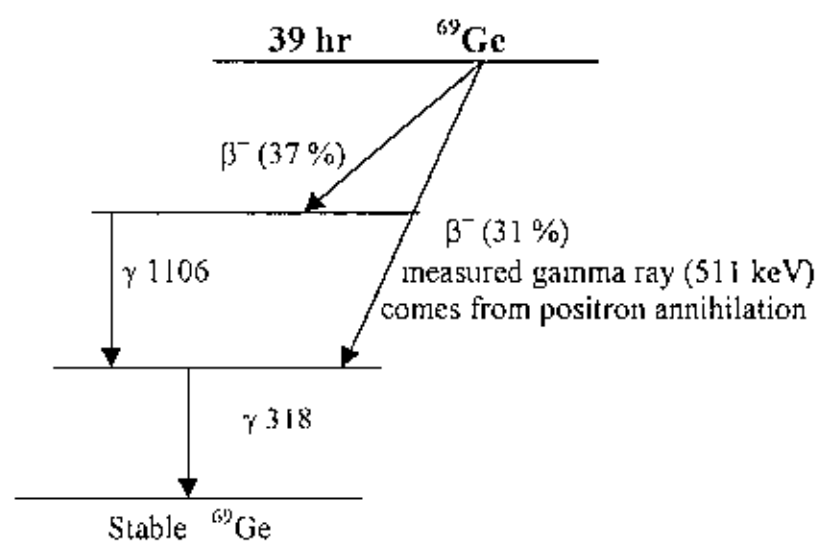


Fig. 4.8. Partial decay scheme of the product nucleus of $^{70}\text{Ge}(n,\alpha)^{69}\text{Ge}$ reaction

CHAPTER 5
NUCLEAR CROSS SECTION CALCULATION
SYSTEM WITH SIMPLIFIED INPUT
FORMAT, VERSION-II (SINCROS-II)

CHAPTER 5

NUCLEAR CROSS SECTION CALCULATION SYSTEM WITH SIMPLIFIED
INPUT FORMAT, VERSION-II (SINCROS-II)

In order to describe the measured cross sections, nuclear model calculations were performed using the computer code SINCROS-II³⁰, which is based on the statistical model, incorporating pre-equilibrium emission. The SINCROS-II has been developed by improving the functions of the program in SINCROS-I⁵⁶ and preparing some process codes for the cross section applications. The input format of this new version is more simplified than that of version I. The level density of nuclei is represented by defining only the Fermi-gas model parameter "a", and "a" for about 200 nuclei were stored in the code as the data initialization statement. The relative widths Γ_γ for 200 nuclei were also stored, although some of them have tentative values

Model calculations using SINCROS-II were done on target nuclides ⁹²Mo, ⁹⁴Mo, ⁹⁶Mo, ⁵⁹Co, ⁹⁰Zr, ⁷⁰Ge, ⁷⁴Ge and ⁷⁶Ge. Neutron, proton and alpha-particle emission was taken into account from every compound nucleus and the necessary data for all nuclei were supplied. In the new version, the total neutron, proton, deuteron, alpha-particle, and gamma-ray production cross sections are shown in the table. Instead of the excited state productions, the isomeric state production cross sections are directly out-putted. It is not necessary, then, to find out the isomeric cross section within the excited state production cross sections. The isomer, of which the excitation function is intended to be given, can be designated in the last row of the input data

In the present experiment, the neutron activation cross section values in the energy range of 13 to 15 MeV were measured theoretically using code SINCROS-II. The theories, models, assumptions and parameters on which SINCROS-II code is based are briefly explained below.

5.1 Composition of SINCROS-II

The main codes of the SINCROS-II are the ELIESE⁵⁷ - GNASH⁵⁸ joint program (EGNASH2) and simplified input version of DWUCK4⁷⁷ (DWUCKY). EGNASH2 calculates the nuclear cross sections over the wide mass region using the built-in optical-model potential parameters. In DWUCKY, the same accepted neutron potentials are programmed as in EGNASH2. The discrete level data--excitation energy, spin, parity and branching ratios of gamma ray decay channels--are prepared from the ENSDF through the format conversion and the editorial work. It is not necessary that too many levels are quoted from the ENSDF, rather it should be assured that the number of levels approximately increases as an exponential function of the excitation energy.

EGNASH2 reads the discrete level data, the direct inelastic scattering cross sections calculated with DWUCKY, and the input data for the nuclear reactions. In addition to the output lists, the results of calculation can be stored into several files which are selected according to the object of calculation. The composition of SINCROS-II and the flow of data processing are shown in Figure 5.1. The particle and gamma-ray total production cross sections and the production cross sections for reaction products, including isomeric states, are held in file 12.

5.2 Input and Output Format of EGNASH2

When we used the GNASH code, the transmission coefficients for neutrons, protons and alpha particles calculated from ELIESE3 were provided as input data to GNASH. Since many of the parameters were predetermined and stored in the program, the parameters which should be inputted are a small number. For the isomeric states, data are given in the last row of the input file.

In addition to the output of the original GNASH, the present code has a table of reaction cross sections to examine the results of calculation as soon as possible. The table includes the compound, direct, rate of pre-equilibrium processes and particles and

gamma-ray total production cross sections. The ground and isomeric states production cross sections of isotopes and level inelastic scattering cross sections are also shown.

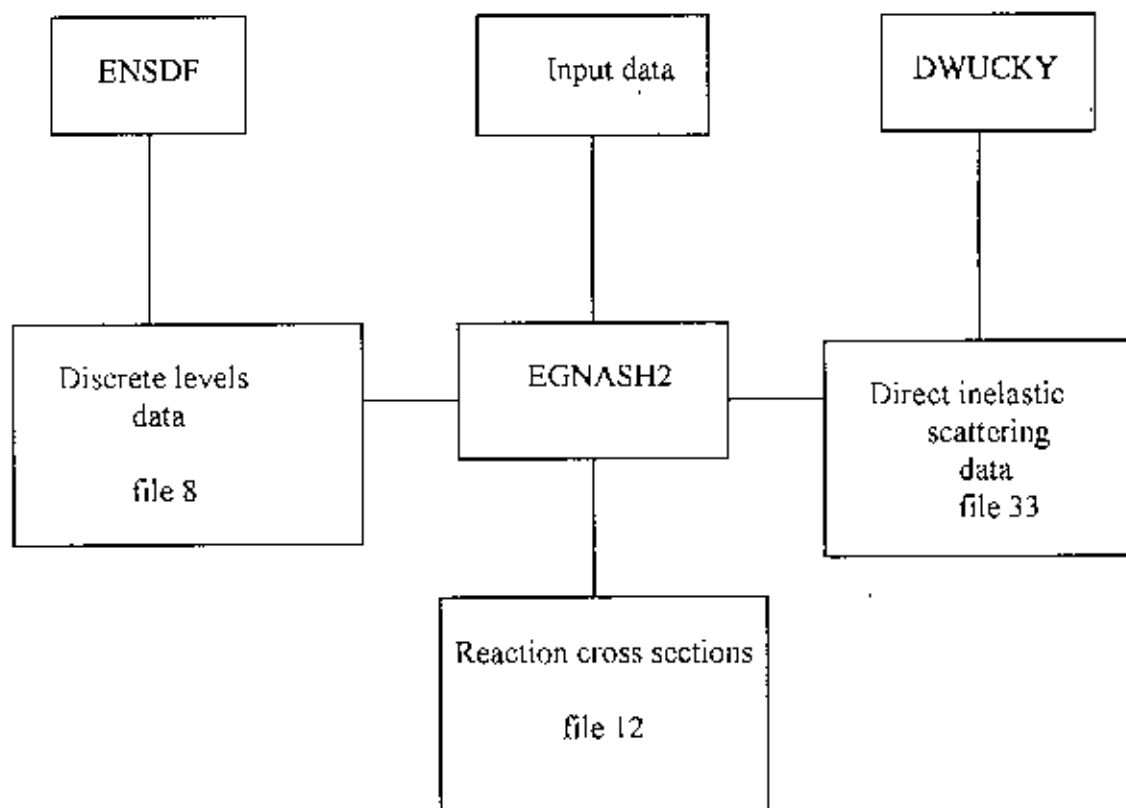


Fig. 5.1. Composition of SINCROS-II and the flow of data processing. Only relevant blocks are shown.

5.3 Optical Model Potential Parameters

A sequential evaporation is assumed for the particles and gamma-rays emitted in the nuclear reactions. Considering the conservation of the angular momentum, parity, each evaporation step is treated within the framework of the statistical model. The particle transmission coefficients are generated using parameters chosen from a global optical-model parameter set. For neutron, the optical model parameter set of Walter-Guss⁵⁹ and Wilmore-Hodgson⁶⁰ are built into the EGNASH2. Walter-Guss recommend their potential to be applied above 53 in mass number and 10 to 80 MeV in energy range.

5.4 Parameters for Level Density and Gamma-ray Transitions

In the continuum level region, the Fermi-gas and the constant temperature model are used to represent the level density of nucleus. The Fermi-gas model formula as a function of energy E and spin J is

$$\rho(E, J) = \frac{\text{Exp}[2\{a(E - \Delta)\}^{1/2}]}{C_0 (E - \Delta)^2} R(J, E) \quad (5.1)$$

where $C_0 = 24\sqrt{2} (0.146)^{1/2} a A$ and the spin term is given by

$$R(J, E) = (2J+1) \exp[-(J+1/2)^2 / \{2\sigma^2(E)\}] \quad (5.2)$$

where $\sigma^2(E)$ is the spin cutoff factor defined by

$$\sigma^2(E) = 0.146 [a(E - \Delta)]^{1/2} A^{2/3} \quad (5.3)$$

The pairing correction Δ was quoted from the Gilbert and Cameron's paper⁶¹. In the lower excitation, the constant temperature formula expressed by

$$\rho(E, J) = \rho(E_\lambda) \exp[(E - E_\lambda)/T] R(J, E), \quad E < E_\lambda, \quad (5.4)$$

is used, where E_λ is the energy at which both densities are smoothly connected and $\rho(E_\lambda)$ is the energy term of level density at the energy E_λ . If the spin dependent level density $\rho(E, J)$ is summed over the spin J , we get the density $\rho(E)$ of levels of all J , which has a different form from the constant temperature formula of Gilbert and Cameron as the spin cutoff factor is energy dependent.

The GNASH code is able to automatically determine the nuclear temperature, T , if the discrete levels in the low energy region and the Fermi-gas level density parameter "a" were suitably inputted. Then the level density of nucleus in the continuum can be described by the parameter "a" only. In some cases, however, the code is unable to match discrete levels, and thus the temperature, which connects smoothly between the Fermi-gas and discrete levels, is not determined. For those cases, the temperature is calculated with a systematic relation between level density parameter and temperature,

$$T = 7.50 a^{-0.84} \quad (5.5)$$

in the code EGNASH2

At the beginning of the calculation, when the experimental value of the average spacing D_0 of s-wave neutron resonance at the neutron binding energy E_B is known⁶², the parameter "a" was assumed to have a value which is calculated from the spacing D_0 by inversely solving the equation⁶³,

$$D_0 = C_0 (E_B - \Delta)/(2I+1) \exp\left[\frac{\{3 + (2I+1)^2\} / \{8\sigma^2(E_B)\} - 2\sqrt{a(E_B - \Delta)}}{a}\right] \quad (5.6)$$

where I is the spin of target nucleus. And a set of parameters "a" of isotopes in the nuclear decaying processes has practically been selected through the cross section calculation to agree with the various experimental data which could be considered to be reliable.

With the cross section calculations for about 50 nuclei, the level density parameters "a" of about 200 isotopes were determined and stored into the EGNASH2 as the data initialization statement. The relation between these "a" and the total shell corrections S is given by Gilberet and Cameron. The tentative formula,

$$a/A = 0.008 S + 0.17 \quad (5.7)$$

is programmed to give the initial value of "a" for the under formed nuclei for which the cross section is not yet calculated. Here S is the shell correction energy.

To provide gamma-ray transmission coefficients, the Brink-Axel giant dipole resonance form was used. The defaulted energy and width of the giant resonance are $E_R = 40 A^{-1/5}$ MeV and $\Gamma_\gamma = 6$ MeV, respectively. The normalization constant is obtained from the ratio of the average radioactive width Γ_γ to the observed resonance spacing D_0 for s-wave neutrons at the neutron binding energy E_B , which is derived in the code from the level density parameter "a" used in the cross section calculation by the formula (5.6).

5.5 Determination of the Value of Parameters

In SINCROS, the global optical-model potential parameters are employed to calculate the transmission coefficients as mentioned in section 5.3. The nonelastic cross sections for neutron and the reaction cross sections for proton calculated with the built-in potentials agreed with experimental data. The key points of the cross section calculation, therefore, are the determination of level density parameters of daughter nuclei and the rate of contribution of pre-equilibrium and direct processes to the statistical process. In the following, the method of parameter determination for the pre-equilibrium process and for the level density is described in detail at subsections 5.5.1 and 5.5.2 respectively.

5.5.1 Parameter Determination of the Pre-equilibrium Process

In the code EGNASH2, the pre-equilibrium and direct processes of particle emission are treated with the code PRECO developed by Kalbach⁶⁴, which is coupled with GNASH, and with the code DWUCKY for the inelastic scattering. In the GNASH, the single particle state density and the normalization factor for excitation-model were free parameters. In contrast with this, the single-particle state density constant is not free, but related to the level density parameter "a" by the formula,

$$g = (6/\pi^2)a \quad (5.8)$$

in the EGNASH2. In addition the normalization factor F2, which is equal to the Kalbach constant divided by 100, the adjusting factors F3 and F4 are introduced for pick-up and knock-out processes, respectively. The factor F2 and the contribution of direct inelastic scattering are so determined that the calculated neutron emission spectrum is in agreement with the high energy part of the experimental neutron spectrum, when the experimental data at 14 MeV are available.

5.5.2 Parameter Determination of the Level Density

After the parameters for the pre-equilibrium and direct processes were selected, the free parameter to be determined is only the level density parameter "a" in the Fermi-gas

model, because the nuclear temperature used in the constant temperature model can be determined automatically or by the equation (5.5). Since the total emission of various kinds of particles from the compound nucleus is controlled by a set of level density parameters for daughter nuclei, it is better that the level density parameter of each daughter nucleus is so practically determined that the calculated cross sections for reactions $(n,2n)$, (n,p) , and (n,α) agree with the experimental data of respective reactions.

The first step to fix the level density parameters is the calculation of them using the experimental value of mean level spacing for s-wave neutron resonance at the neutron binding energy. The calculation was made by solving inversely equation (5.6), with the spin cutoff-factor defined by equation (5.3) and the pairing correction quoted from Gilbert and Cameron.

The second step to determine the level density parameters is the cross section calculation in the mass region where the reliable experimental data exist. Several test calculations of cross sections around 14 MeV were carried out, referring to the experimental data for the $(n,2n)$, (n,p) , and (n,α) reactions. In this stage, the measurements of cross sections of Mo isotopes performed by Ikeda et al. and Katoh et al. are very useful for the determination of level density parameters.

CHAPTER 6
RESULTS AND DISCUSSION

CHAPTER 6

RESULTS AND DISCUSSION

Cross sections for a total number of eight (n,2n), (n,p) and (n, α) reactions on the isotopes of molybdenum, cobalt, zirconium and germanium were measured in the neutron energy range 13.90 - 14.80 MeV. The measured cross sections along with the literature data and the calculated values produced by SINCROS-II are plotted using software Sigma Plot and presented in Figures 6.1-6.8. The results of the eight reactions are discussed in the subsequent sections.

6.1 The $^{92}\text{Mo}(n,p)^{92m}\text{Nb}$, $^{94}\text{Mo}(n,2n)^{93m}\text{Mo}$ and $^{96}\text{Mo}(n,p)^{96}\text{Nb}$ Reactions

The activation cross sections including error obtained from the present investigation for $^{92}\text{Mo}(n,p)^{92m}\text{Nb}$, $^{94}\text{Mo}(n,2n)^{93m}\text{Mo}$ and $^{96}\text{Mo}(n,p)^{96}\text{Nb}$ reactions at the neutron energy 14.80 MeV are given in Table 4.4. Each cross section value is based on three independent measurements.

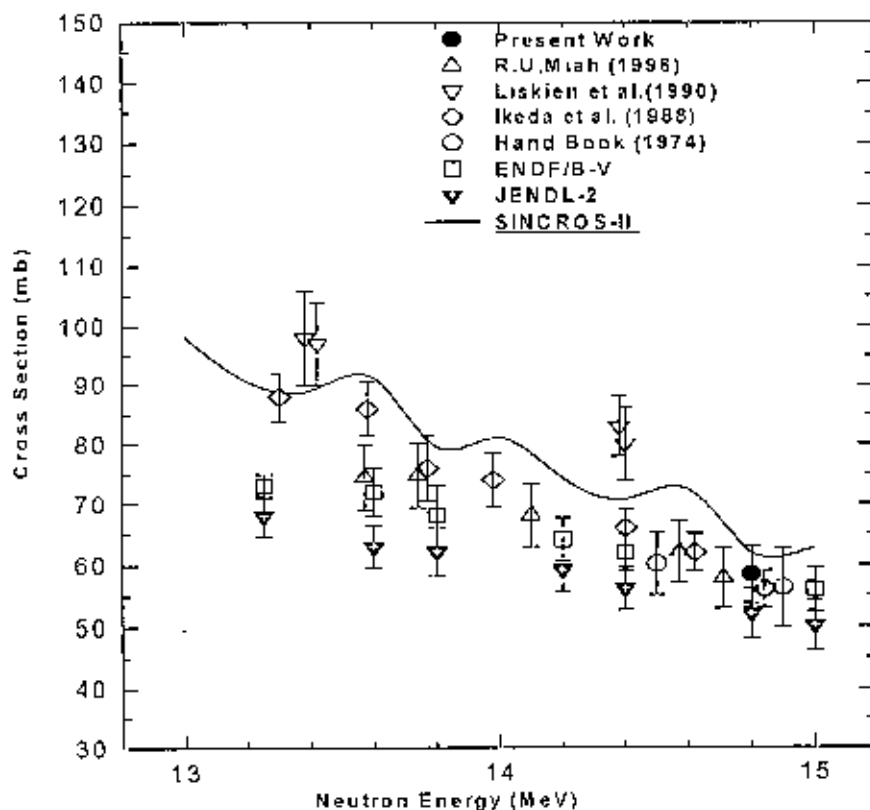


Fig 6.1. The activation cross section of the $^{92}\text{Mo}(n,p)^{92m}\text{Nb}$ reaction.

The present experimental cross section of reaction $^{92}\text{Mo}(n,p)^{92\text{m}}\text{Nb}$ and the literature data are shown in Figure 6.1. Liskien et al.⁶⁵ has measured the cross sections of this reaction but their reported values are 24–35% higher than ENDF/B-5⁶⁶ and 39–41% higher than JENDL-2⁶⁷ values. The cross section data for this reaction obtained from the present investigation are in fairly good agreement with the results obtained from the nuclear model calculations using the latest computer code SINCROS-II³⁰, ENDF/B-5, JENDL-2 and also with the results obtained by Ikeda et al.²⁴.

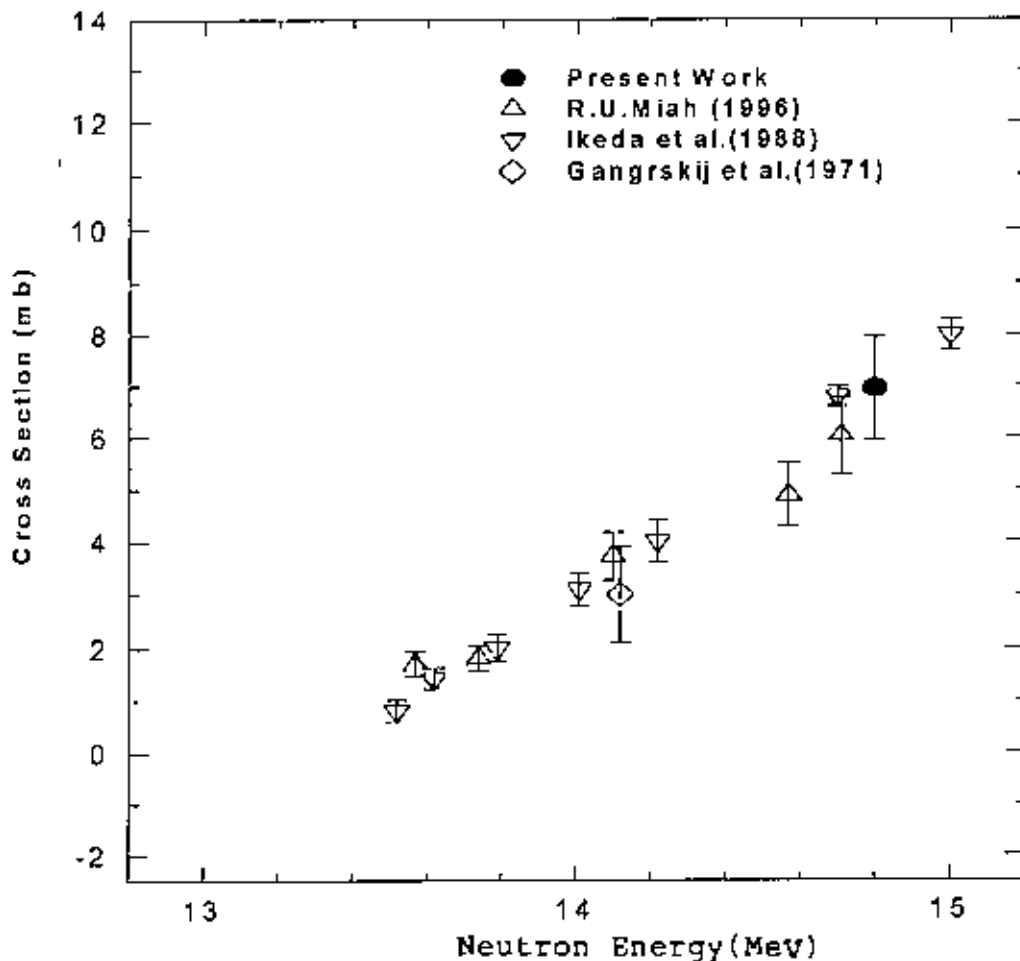


Fig.6.2. The activation cross section of the $^{94}\text{Mo}(n,2n)^{93\text{m}}\text{Mo}$ reaction.

Extremely few published^{19,24,65} experimental cross section data of $^{94}\text{Mo}(n,2n)^{93\text{m}}\text{Mo}$ reaction are available. More experiments are needed to give precision cross section data of this reaction. Measured data with literature are shown in Figure 6.2, as a function of neutron energy. The present experiments introduce newer data point to the existing literature. The literature values are very close to our measured cross section and are in good agreement.

The cross section of the reaction $^{96}\text{Mo}(n,p)^{96}\text{Nb}$ along with the other literature data are shown as a function of neutron energy in Figure 6.3. Although, activation cross sections data of this reaction are abundant^{24,68,65,69,19,30} in literature, the discrepancies of some reported cross section data need further investigation. The measured data gives good agreement with Ikeda et al.²⁴ and Miah¹⁹.

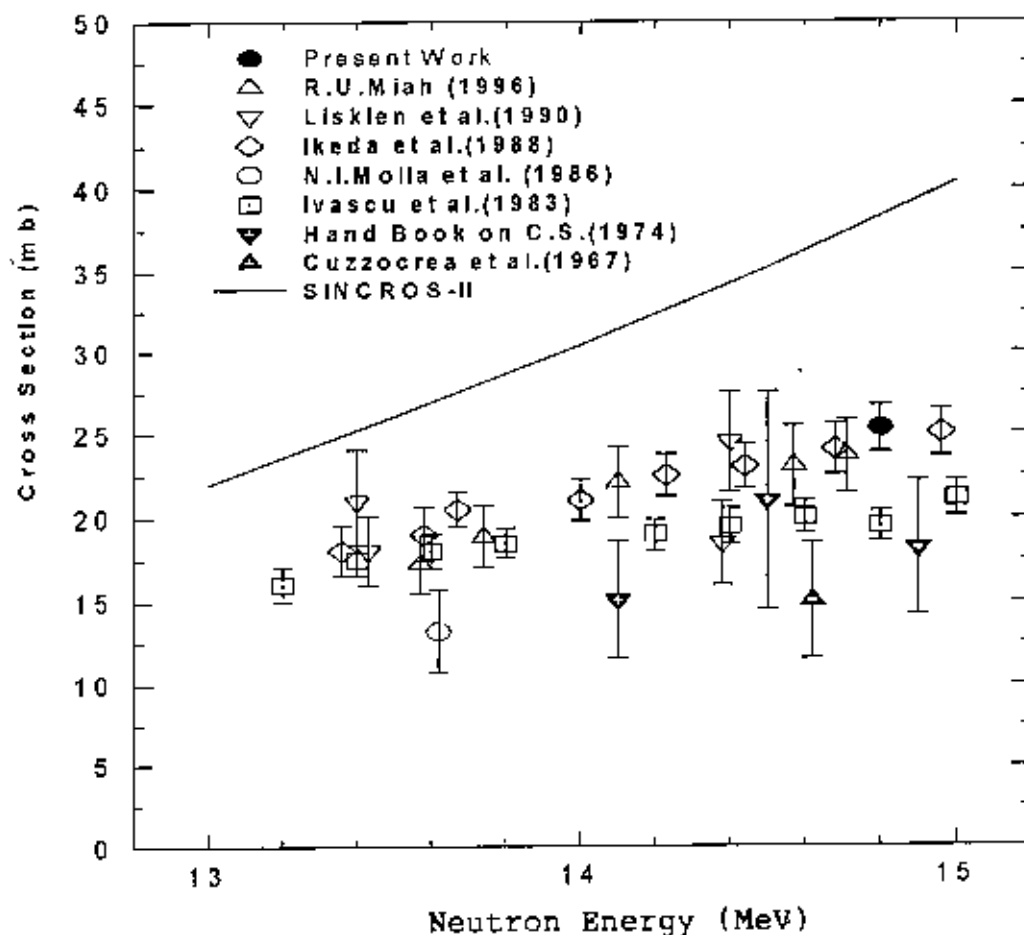


Fig.6.3. The activation cross section of the $^{96}\text{Mo}(n,p)^{96}\text{Nb}$ reaction.

6.2 The $^{59}\text{Co}(n,\alpha)^{56}\text{Mn}$ Reaction

Activation cross section data in the neutron energy 14.80 MeV for the reaction $^{59}\text{Co}(n,\alpha)^{56}\text{Mn}$ are scarce. So it was necessary to conduct experiment to measure cross section for this reaction. The measured data along with literature values are shown in Figure 6.4. Our data is higher than those of Liskein et al.⁷⁰ but close to theoretical values obtained using statistical code SINCROS-II.

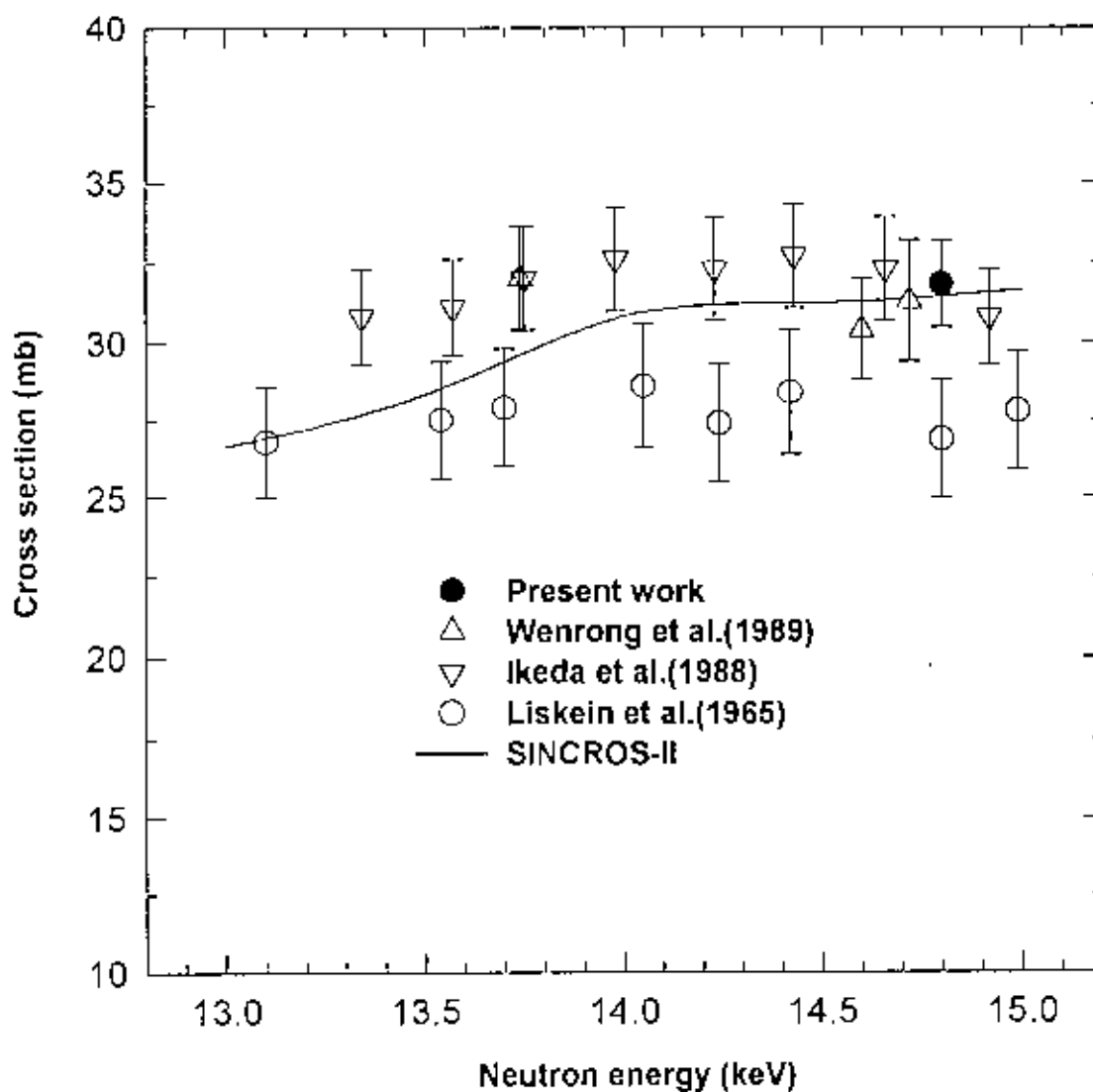


Fig.6.4. The activation cross section of the $^{59}\text{Co}(n, \alpha)^{56}\text{Mn}$ reaction.

6.3 The $^{90}\text{Zr}(n,2n)^{89}\text{Zr}$ Reaction

The measured cross sections including errors obtained from the present investigated $^{90}\text{Zr}(n,2n)^{89}\text{Zr}$ reaction in the neutron energy range 14.10-14.71 MeV are given in Table 4.4. The values obtained from this work, literature data^{1,24,71,25,19,72} and the values obtained via model calculation with statistical code SINCROS-II are shown in Figure 6.5 as a function of neutron energy. The large discrepancy in the nuclear model

calculation using SINCROS-II code is observed for the investigated reaction. The model consists of a pure multistep approach with the fixed global parameter set. It contains both statistical multistep direct and statistical multistep compound processes. The probable reason of large discrepancy in the cross section estimations via this code is that the compound nucleus formation cross section is underestimated in SINCROS-II whereas direct reaction is overestimated. It is worth mentioning that the measured excitation function for $^{90}\text{Zr}(n,2n)^{89}\text{Zr}$ reaction is in good agreement with the literature values. The present work introduces some newer data points to the existing literature and theoretical calculation.

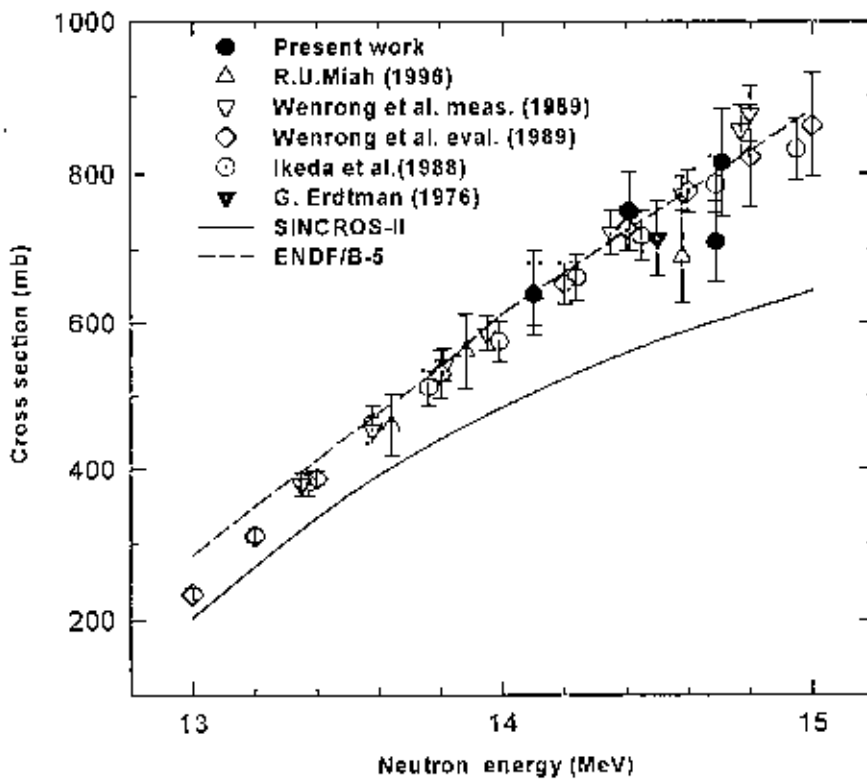


Fig.6.5. The excitation function of $^{90}\text{Zr}(n,2n)^{89}\text{Zr}$ reaction.

6.4 The $^{70}\text{Ge}(n,2n)^{69}\text{Ge}$ Reaction

The cross section values as a function of neutron energy obtained from the present investigation along with literature data for $^{70}\text{Ge}(n,2n)^{69}\text{Ge}$ reaction have been shown in Figure 6.6. The results of the nuclear model calculation are also shown as a curve along with the measured values. The quoted uncertainty in each cross section value includes both statistical and systematic errors. The total uncertainties in the cross section values are in the range 7 - 9%

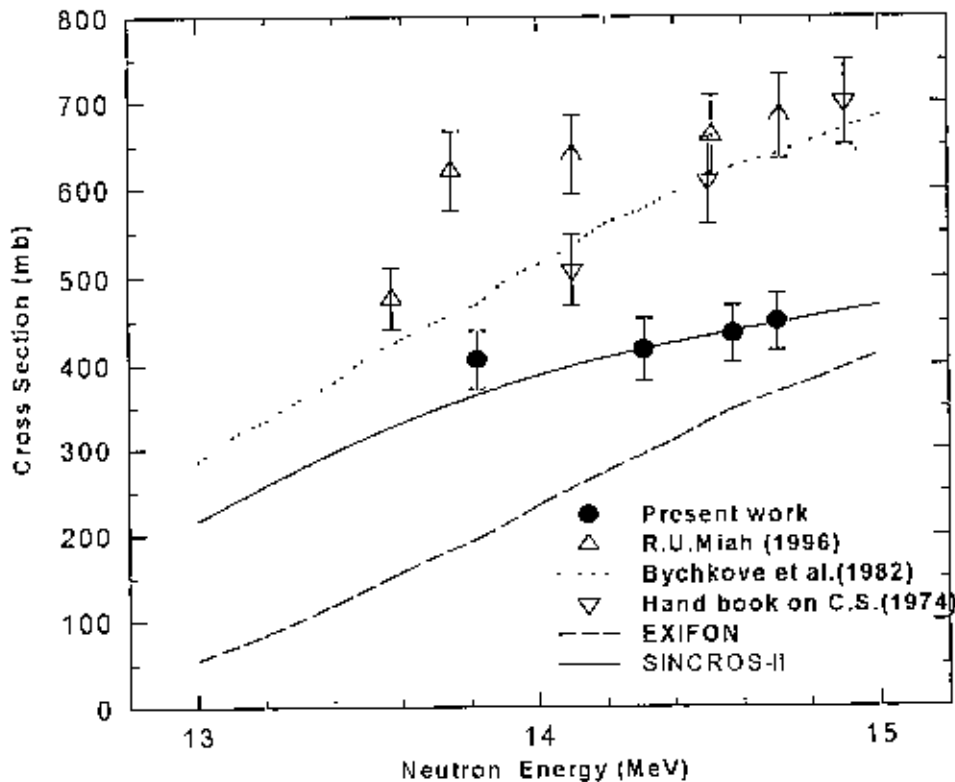


Fig.6.6. The excitation function of the $^{70}\text{Ge}(n,2n)^{69}\text{Ge}$ reaction.

From the figure 6.6 it is observed that the theoretical values obtained by using the code SINCROS-II are very close to our measured cross section and are in good agreement. The present values are above the values obtained via EXIFON. The large discrepancy in the nuclear model calculation using SINCROS-II and EXIFON codes is observed.

for the investigated reaction in the neutron energy range 13 –14 MeV. The model consists of a pure multistep approach with the fixed global parameter set. It contains both statistical multistep direct (SMD) and statistical multistep compound (SMC) processes. The probable reason of large discrepancy in the cross section estimations via this code is that the compound nucleus formation cross section is underestimated in SINCROS-II whereas direct reaction is overestimated. The results obtained from the work of R.U Miah¹⁹, Bychkov²³ et al, and the values obtained from Hand Book⁶⁸ at 14.5, 14.9 MeV energies are clearly larger than the present result. It may be mentioned that the measured data of present work is in excellent agreement with the results obtained from the nuclear model calculations using the latest computer code SINCROS-II.

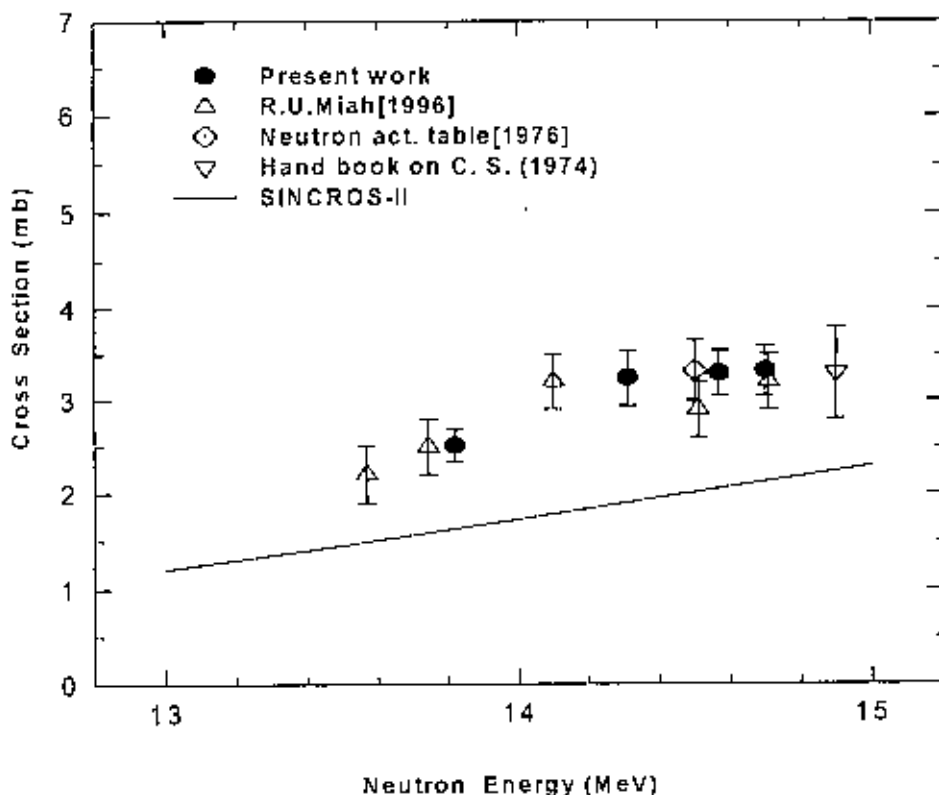


Fig.6.7. The Excitation Function of the $^{74}\text{Ge} (n, \alpha) ^{71m}\text{Zn}$ Reaction.

6.5 The $^{74}\text{Ge}(n,\alpha)^{71m}\text{Zn}$ Reaction

The activation cross sections measured in the present work for the $^{74}\text{Ge}(n,\alpha)^{71m}\text{Zn}$ reaction in the neutron energy range 13.82- 14.70 MeV are summarized in Table 4.4 together with the error limit. Over the energy range investigated in this work^{25,68,77-76}, a very few cross section data exist in the literature and there are large discrepancies among them. The present data were compared with the previously reported values as well as with the theoretical values are shown in Figure 6.7. The present results are larger than that of the theoretical values obtained from the statistical code SINCROS-II¹⁵. It is worth mentioning that the measured excitation function for $^{74}\text{Ge}(n,\alpha)^{71m}\text{Zn}$ reaction is in good agreement with the literature values^[65,8,10].

6.6 The $^{76}\text{Ge}(n,2n)^{75m+g}\text{Ge}$ Reaction

Extremely few published experimental cross section data of $^{76}\text{Ge}(n,2n)^{75m+g}\text{Ge}$ reaction are available and there exist large discrepancies among them that demand more experiment to give reliable data. The measured data with literature are shown in Fig. 6.8 as a function of neutron energy. The results of the nuclear model calculation using statistical code EXIFON performed earlier in our laboratory¹⁹ are also shown in Figure 6.8. All the measured values give the cumulative cross section for the formation of the ground state. Since the metastable state could not be measured due to its short half life of 48.9 seconds, a correction for its contribution to the cumulative cross section could not be estimated. We therefore calculated cross sections for the independent formation of the two isomeric states and obtained the cumulative cross section for ^{75}Ge . The present data are lower than those of R. U. Miah. Our measured data are well supported by S. Okumura⁷⁷ and G. Erdtman²⁵. Our measured data is close to that of the data evaluated by Bychkov et al²³, and ~ 5 % higher than those of theoretical calculation. There appears to be a good agreement between the experimental results and the theoretical results.

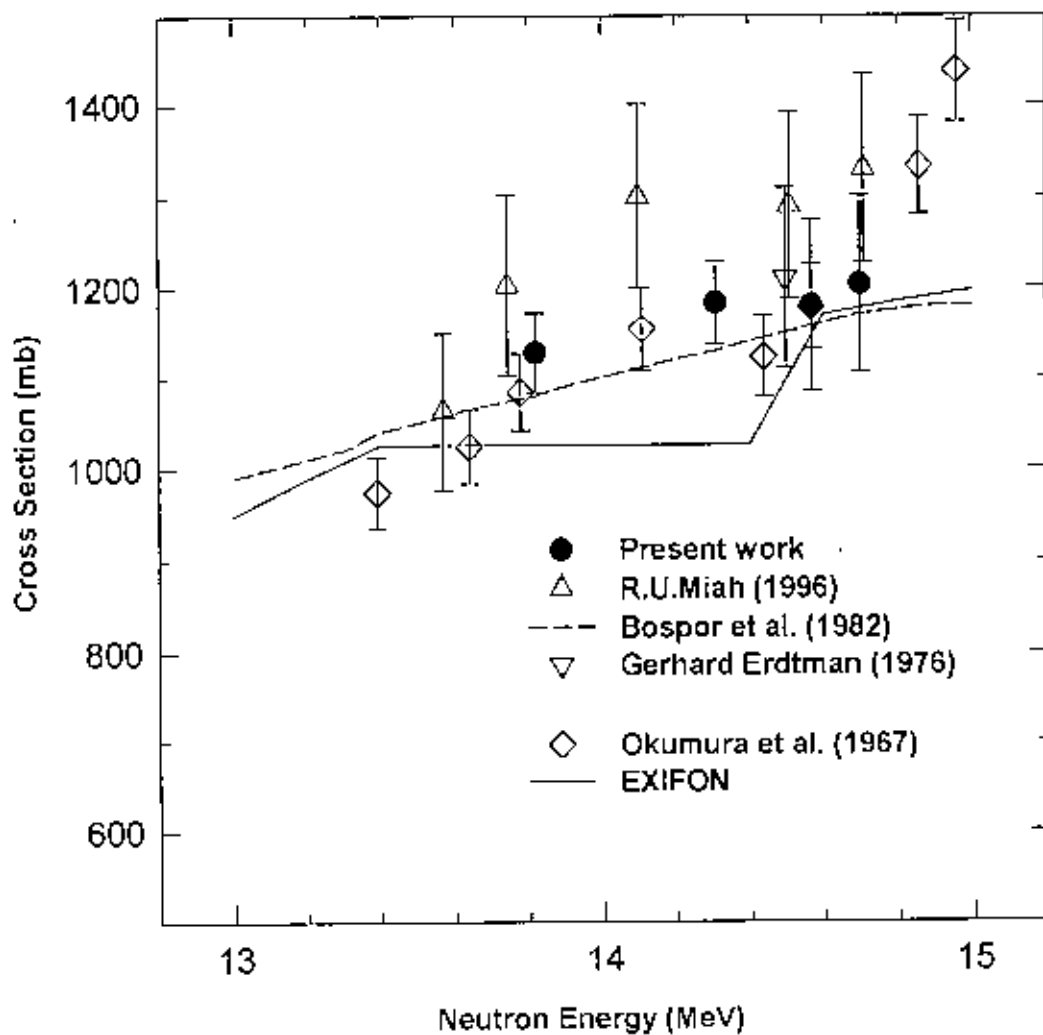


Fig.6.8. The excitation function of the $^{76}\text{Ge}(n, 2n)^{75m+g}\text{Ge}$ reaction.

CHAPTER 7
REFERENCES

REFERENCES

1. R. Wolffe and S. M. Qaim, *J. Radi. Acta* **27**, 65-69 (1980)
2. J. Csikai, Proc. advisor group meeting on nuclear data for fusion reactor technology, Viena (1978), IAEA-TECDOC-223, 199 (1979)
3. V.M. Bychkov, V.N. Manokhin, A.B. Pashchenko, V.I. Plyaskin, Report INDC(CCP)-146 / LJ, 1-149 (1980)
4. E. Steiner, P. Huber, W. Salathe and R. Wagner, *Hel. Phys. Acta* **43**, 17 (1970)
5. D. J. Rose and R. Carruthers, Proc. of an IAEA Workshop Culham, United Kingdom, 3,9, 29 Jan.-15 Feb (1974)
6. F.H. Tenney, Proc. of an IAEA Workshop Culham, United Kingdom, 17, 29 Jan.-15 Feb. (1974)
7. Y. Seki and T. Hiraoka, in preparation
8. K. Sako, M. Ohta, Y. Seki, H. Yamato, T. Hiraoka, K. Tanaka, N. Asami and S. Mori, Proc. of an IAEA Workshop Culham, United Kingdom, 27, 29 Jan.-15 Feb. (1974).
9. J.T.E. Nihoul, S.C.K.-C.E.N., Mol, Belgium, Proc. of a Symposium, VIENNA, 2-6 June (1969).
10. R. Vojan, *Phys. Stat. Sol.* **6**, 925 (1964), **7**, 299 (1964); and **8**, 331 (1965)
11. W. Kohler and W. Schilling, *Nukleonik* **71**, 384 (1965).
12. G. Burger et al, *Phys. Stat. Sol.* **4**, 281 (1964)
13. K. Dettmann, *Phys. Stat. Sol.* **10**, 269 (1965).
14. G. Luck and R. Sizmann, *Phys. Stat. Sol.* **5**, 683 (1964).
15. M. Balarin and O. Havser, *Phys. Stat. Sol.* **10**, 475 (1965).
16. G.W. Iseler et al, *Phys. Rev.* **146**, 468 (1966).
17. Status reviews of 14 MeV neutron induced cross sections, measurements and calculations, INDC(NDS)-173/GJ, IAEA Nuclear data section, Vienna Sept. (1985).
18. N. Banu, M.Sc Thesis, Dept. of Physics, Jahangirnagar University (1999).
19. R.U. Miah, Ph.D Thesis, Dhaka University (1996).
20. H. Kalka, A model for statistical multistep reactions (code EXIFON) INDC(GDR)-060/L, Sept. (1990)

- 21 M. Belgaid and M. Asghar, *J. App. Radi. And Isotopes* 49(12), 1497-1503, Dec. (1998).
- 22 D.E. Cullen, N. Kocherov, P.K. McLaughlen, IRDF[9], Internal report, IAEA-NDS-48, IAEA, Vienna (1982).
- 23 V.M. Bychkov, K.I. Zolotarey, A.B. Pashchenko, V.I. Plyaskin, Rept. INDC (CCP)-183/L (1982).
- 24 Ikeda et al., JAERI-1312 (1988)
- 25 G. Erdtman, *Neutron Act. Tables, Kernchemie in Einzeldarstellungen* 6 (1976).
- 26 S. M. Qaim and Stocklin, Proc. Int. Conf. Organized by the British nuclear energy society held on 20-22 Sept. 1971.
- 27 V. S. Rao and J. R. Rao, Proc. Int. Conf. on nuclear cross-section for technology, Knoxville, Tenn., 22-26 Oct. (1979) published as NBS special pub. 594 (1980).
- 28 CINDA, 1982 (EXFOR-10751.002, March 1979).
- 29 Y. Fujino, M. Hyakutake and I. Kumabe, NEANDC(J)-52/U (1977).
- 30 N. Yamamuro, A Nuclear Cross Section Calculation System with Simplified Input Format, Version-II, SINCROS-II, JAERI-M, 90-006, NEANDC (J)-146/U, INDC (JPN)-133/L. Feb. (1990).
- 31 B.K. Sharma, *Instrumental method of analysis* 219, 14th ed. (1994).
- 32 Proc. of specialist's meeting on nuclear data for fusion neutronics, JAERI-M 86-029, Japan atomic energy research inst., March (1986)
- 33 *Handbook on nuclear activation data*, IAEA, Vienna, Technical report series no273.
- 34 J.C. Laul, *Neutron activation analysis of geological materials*, Atomic energy review 17 2 (1979).
- 35 S. Nargolwalla and E.P. Przybylowicz, *Activation analysis with neutron generators*, 23, John Wiley and Sons, New York (1973)
- 36 S. Cierjacks (editor), *Neutron sources for basic physics and applications*, Pergamon press (1983).
- 37 J. Csikai, *Handbook of fast neutron generators*, Vol. I, CRC Press, Inc. (1987).
- 38 S. Glastone and A. Sesonske, *Nuclear reactor eng.*, 3rd ed., CBS publisher and distributors, Dhelhi (1986)
- 39 *Manual of troubleshooting and upgrading of neutron generators*, IAEA-TECDOC-913, International atomic energy agency, Nov (1996).

- 40 Certificate of tritium source, Radioisotope center, POLATOM, Poland
- 41 G.F. Knoll, Radiation detection and measurement, 2nd ed, John Wiley and Sons, New York (1989).
42. H.J. Arnikar, Essentials of nuclear chemistry, 318, 4th ed, Jan. (1995).
43. I Kaplan, Nuclear physics, 411, 2nd ed., copyright (1962)
44. S.S. Kapoor and V.S. Ramamurthy, Nuclear radiation detectors, Wiley Eastern limited, New Delhi (1986)
- 45 H A. Enge, Introduction to nuclear physics.
46. CANBERRA Product catalogue, 4, 10th ed, Addition Wisely.
47. A P Malvino, Electronic principles, Tata McGraw-Hill publishing company limited, New Delhi (1984).
- 48 D. De Soete, R. Gijbels and J. Hoste, Neutron activation analysis, John Wiley, New York (1972).
49. G Bertolini and A. Coche, Semiconductor detectors, North-Holand, Amsterdam (1968)
50. CANBERRA Germanium detectors, User's Manual (1991).
51. H. Vonach, Nuclear data standards for nuclear measurements, Technical report series 227, 59 IAEA (1983).
- 52 Cart of the Nuclide, Knolls Atomic Power Laboratory, operated by the General Electric Company under direction of Naval Reactors, U S Department of Energy, 14th ed., Apr. (1988).
53. Lederer, Hollander, Herlman, Table of Isotopes, 6th ed., John Wiley and Sons
54. R.L. Health, Gamma-ray spectrum catalogue, Ge and Si detector spectra, 4th ed., Original work published- March (1974), Electronic version with updated nuclear data and decay schemes added Sept (1998)
55. G. Friedlander, J.W. Kenneday, E.S. Macias and J.M. Miller, Nuclear and radiochemistry, 610, 3rd ed. (1981).
- 56 N Yamamuro, A nuclear cross section calculation system with simplified Input-Format Version-I (SINCROS-I), JAERI-M, 88-140 (1988).
57. S. Igarashi, Program ELIESE-3 ; Program for calculation of the nuclear cross section by using local and non-local optical models and statistical model, JAERI 1224 (1977).

58. P.G. Young and D.D. Arner, GNASH ; A preequilibrium, Statistical nuclear- model code for calculation of cross sections and emission spectra, LA-6947 (1977).
59. R.L. Walter and P.P. Guss, A global optical model for neutron scattering for $A > 53$ and $10 \text{ MeV} < E < 80 \text{ MeV}$. Proc. Int. Conf., Nuclear data for basic and applied sciences, Santa Fe, New Mexico, 1079 (1985).
60. D. Wilmore and P.E. Hodgson, Nucl Phys **55**, 673 (1964).
61. A. Gilbert and A.G.W. Cameron, Can J Phys, **43**, 1446 (1965).
62. S.F. Mughabghab, M. Divadecnam and N.E. Holden, Neutron cross sections 1, Neutron resonance parameters and thermal cross sections, Part A, Z= 1-60 (1981).
63. S. Ijima, T. Yoshida, T. Aoki, T. Watanabe and M. Sasaki, J Nucl Sci Tech. **10**, 21 (1984)
64. C. Kalbach, Z Physik, **A 283**, 401 (1977)
65. H. Liskien, R. Wolffe, R. Widera and S. M. Qaim, *Appl. Radiat. Isot.*, **41**(1) (1990).
66. R. Kinsey, Evaluated nuclear data file, ENDF/B-V, ENDF/B. Summary documentation, ENDF-201, 3rd edition, Brook haven national laboratory, (1979).
67. T. Nakagawa, Summary JENDLE-2 general purpose file, JAERI-M 84-103 (1984).
68. Hand book on nuclear activation cross sections, Technical report series no. 156, IAEA, Vienna (1974).
69. V. Lvascu, Nuclear model calculations of (n,p) and (n,n'p) reactions on molybdenum isotopes, Nucl. Phys. **28** (1983).
70. H. Liskien and A. Paulsen, J. Nucl Energy AB **19**, 73 (1965).
71. Z. Wenrong, L. Hanlin, Y. Weixiang and Y. Xialin, INDC (CPR)-16 (1989).
72. C. Philis, Dosimetry data file ENDF/B-5 (1979).
73. V. M. Bychkov, V. N. Manokhin, A. B. Pashchenko and V. I. Playskin, Cross section for the (n,p), (n, α) and (n,2n) threshold reactions, Rcp INDC (CCP)-146/LJ (1980).
74. S. M. Qaim, Nucl. Phys **A185**, 614 (1972)
75. L. A. Rayburn, Phys Rev **122**, 168 (1961).
76. R. Rieppo, Keinanen and Volkonen, J. Inorg Nucl. Chem. **38**, 1927 (1976).
77. S. Okumura, Nucl. Phys **74**, A93 (1967).

APPENDICES

APPENDICES

Summary

In the present experiment, the cross sections of $(n,2n)$, (n,p) and (n,α) reactions on the isotopes of molybdenum, cobalt, zirconium and germanium were determined through identification of the activation products via γ -ray spectrometry.

Samples of molybdenum(as Mo_2O_3) and germanium metal powder in the form of pellet with dimension of 1.2 cm diameter and ~0.15 cm thickness, zirconium foil of 1cm \times 1 cm were prepared. All of the samples were sandwiched between Al-foils of the same size of sample separately. Aluminium foils were used to measure the neutron flux at the sample positions

One molybdenum and one cobalt sample with Al-foils were irradiated by neutrons at the surface of tritium target over a period of 1.5 hrs. Neutrons were produced at the J-25 Neutron Generator of the Institute of Nuclear Science and Technology, AERE, Savar, Dhaka via $^3\text{H}(d,n)^4\text{He}$ reaction with 110 keV deuterons of 120 μA beam current.

Four zirconium samples were irradiated by neutrons at 0° , 20° , 60° and 90° with respect to the deuteron beam direction. In these cases, the neutron generator operation parameters were beam current 130 μA , deuteron energy 110 keV and irradiation time 3.5 hours. Four germanium samples were also irradiated by neutron for 3.5 hours in the same experimental configuration. The angular positions for germanium samples were 10° , 40° , 70° , 110° with respect to deuteron beam of 110 keV energy and 130 μA current

After irradiation, the radioactivities of the reaction products were measured by using a high resolution HPGe-detector. The gamma-ray spectra were accumulated and analyzed in Canberra S-100 Multi Channel Analyzer (MCA) master board package based on personal computer. The measured counts under photo peak were subjected to usual correction for dead time loss, pileup loss, coincidence effects etc. The background

correction was performed for 909.1 keV gamma-ray energy emitted from the product nuclide ^{89}Zr .

The count rates were converted to decay rates by well known equation shown in previous section. From the decay rates, the cross sections were determined using well known activation formula that are shown in section 4.1. The uncertainty in cross sections were determined by considering both the systematic and statistical errors. The overall uncertainties for the present work were in the range of 3-8 %. The maximum errors in the cross sections are due to the poor counting statistics.

The cross sections of the $^{92}\text{Mo}(n,p)^{92m}\text{Nb}$, $^{94}\text{Mo}(n,2n)^{93m}\text{Mo}$, $^{96}\text{Mo}(n,p)^{96}\text{Nb}$ and $^{59}\text{Co}(n,\alpha)^{56}\text{Mn}$ reactions were measured at 14.80 MeV neutron energies. The cross sections of the $^{70}\text{Ge}(n,2n)^{69}\text{Ge}$, $^{74}\text{Ge}(n,\alpha)^{71m}\text{Zn}$ and $^{76}\text{Ge}(n,2n)^{75m+g}\text{Ge}$ reactions were measured at 13.90, 14.31, 14.57 and 14.70 MeV neutron energies. The cross sections at 14.10, 14.41, 14.69 and 14.71 MeV neutron energies for $^{90}\text{Zr}(n,2n)^{89}\text{Zr}$ reaction was measured in the same experimental configuration.

The measured cross sections along with the values obtained from available literature were plotted as a function of neutron energy. In the present investigation it is observed that the cross sections of all the (n,2n) reactions on the isotopes increase with the increasing of neutron energy. Whereas the cross section of (n,p) reaction decreases with the increasing of neutron energy.

In order to describe the measured excitation functions of the selected reactions, theoretical calculations of the cross section have been done using the statistical code SINCROS-II in the range of 13-15 MeV neutron energy for four(4) elements in the mass region $A=59-96$.

Up to now, there have been very limited numbers of available data for the activation cross sections of $^{92}\text{Mo}(n,p)^{92m}\text{Nb}$, $^{94}\text{Mo}(n,2n)^{93m}\text{Mo}$, $^{96}\text{Mo}(n,p)^{96}\text{Nb}$, $^{59}\text{Co}(n,\alpha)^{56}\text{Mn}$, $^{90}\text{Zr}(n,2n)^{89}\text{Zr}$, $^{70}\text{Ge}(n,2n)^{69}\text{Ge}$, $^{74}\text{Ge}(n,\alpha)^{71m}\text{Zn}$ and $^{76}\text{Ge}(n,2n)^{75m+g}\text{Ge}$ reactions even at 14 MeV. The cross section data of these reactions measured in present work showed

significant improvement in accuracy in comparison with previously reported data. Hence, the cross section data obtained from the present investigation based on unified experimental condition have provided nuclear database and removed large previous discrepancies for some of the reactions in the energy range of 13.90 to 14.80 MeV. The agreement between experiment and theory is fairly satisfactory in most of the cases.

It is hoped that our measured and calculated cross section data provide real data base for fusion reactor technology design, semiconductor technology development, new evaluations of activation cross sections and to a detailed future theoretical calculation and testing nuclear models.

Error Calculation

The errors in measured cross section values were determined considering both systematic and statistical errors. The systematic errors of the investigated reactions are given in Table 4.4. As an example, the error calculation only for $^{92}\text{Mo}(n,p)^{92\text{m}}\text{Nb}$ reaction at 14.80 MeV is shown below.

Total error in quadrature = $[(\text{statistical error})^2 + (\text{systematic error})^2]^{1/2}$

The statistical error is given by

$$E_{\sigma} = \sqrt{\frac{(\sigma_i - \bar{\sigma})}{N-1}}$$

Where, σ_i = Cross section value

$\bar{\sigma}$ = Average cross section

N = Number of cross section values

We have taken three cross section values from three times counting and obtained statistical error 7.58 % for the cross section 58.37 mb at 14.80 MeV neutron energy

Systematic error

$$= [(0.5)^2 + (0.2)^2 + (0.5)^2 + (1.5)^2 + (1)^2 + (0.5)^2 + (0.5)^2 + (0.3)^2 + (0.2)^2 + (0.5)^2]^{1/2}$$

$$= 2.161 \%$$

$$\text{Total error} = [(7.58)^2 + (2.161)^2]^{1/2}$$

$$= 7.88 \%$$

$$\text{Error for 58.37 mb} = \frac{58.37}{100} \times 7.88$$

$$= 4.6 \text{ mb}$$

For all of the investigated reactions, the similar procedure was followed to determine errors in measured cross section values of the selected neutron energy.

List of Papers Accepted and Communicated for Publication Based on the Present Work

1. M. A. Halim, M. A. Hafiz, K. Naher, R. U. Mia and M. Rafique Ullah, Excitation function of the $^{74}\text{Ge}(n,\alpha)^{71\text{m}}\text{Zn}$ Reaction in the Energy Range 13.90 –14.70 MeV, Journal of Nuclear Science and Application (Accepted)
2. M. A. Halim, M. M. Hossain, R. U. Mia and M. Rafique Ullah, Measurement of the $^{92}\text{Mo}(n,p)^{92\text{m}}\text{Nb}$, $^{94}\text{Mo}(n,2n)^{93\text{m}}\text{Mo}$ and $^{96}\text{Mo}(n,p)^{96}\text{Nb}$ Reactions Cross Sections at 14.80 MeV Neutron Energy, Jahangirnagar University Journal of Science (Communicated).
3. M. A. Halim, M. A. Hafiz, K. Naher, R. U. Mia and M. Rafique Ullah, Cross Sections of the $^{90}\text{Zr}(n,2n)^{89}\text{Zr}$ Reaction in the Energy Range 14.10 –14.71 MeV, Journal of the Bangladesh Chemical Society (Communicated).

